Tampere University

Hans Porras

ELECTROMAGNETIC FORCES CAUSED BY ECCENTRICITIES IN PERMANENT MAGNET MACHINES

Master of Science Thesis
Faculty of Information Technology and Communication Sciences
Examiners: Paavo Rasilo, Umair Ahmed
May 2022

ABSTRACT

Hans Porras: Electromagnetic forces caused by eccentricities in permanent magnet machines
Master of Science Thesis
Tampere University
Master's Degree Program in Electrical engineering
May 2022

Eccentricities cause forces and excitations in electrical machines. These forces result in excessive wear and a reduction in the operational lifetime of the machine. Thus, it is necessary to model them to prevent these conditions and reduce the effects. This thesis was done at Yaskawa Lappeenranta. The scope of this thesis was to model forces caused by different eccentricities and verify the usability of 3D-FEM modelling for the company's purposes. Furthermore, a simple analytical model was created to calculate axial forces. The FEM models made during this thesis were the first 3D models used to calculate the electrical properties of machines within the company, thus providing new knowledge of their machines' operation.

Yaskawa Lappeenranta uses Altair Flux software for their electromagnetic calculations. Therefore, it was selected as the program to model the machines. Two machine types were selected for this study, PMM500 and PMM1500, where the former represents an embedded magnet machine and the latter a surface magnet machine. Selected machines were modelled with radial 2D and 3D models. Actual machine geometries were followed closely, and the materials were selected from Flux's and Yaskawa's libraries. Due to technical restrictions, complete machines could not be fully modelled, and only models with a few partial stacks were created. It was found that some of the forces do not follow a linear increase concerning the number of stator stacks, which is a severe flaw in the practical usability of the program. High calculation times also pose a significant drawback for the practical usability of 3D modelling to calculate the electromagnetic properties of the machines.

Radial forces were modelled only with 2D-FEM models. Radial eccentricity's main result is the increase of the DC component of radial force due to a change in permeance across the machine's air gap. The DC-component increases linearly, concerning eccentricity, and as the force increases, harmonic components from two different sources could be seen. Harmonic components caused by stator slotting could be seen on both the radial forces and the cogging torques. Eccentricity creates harmonic components whose orders are multiples of pole numbers for both machines' cogging torques. Additionally, eccentricity induced a low order harmonic component to the PMM500's radial force. No significant result can be concluded for eccentricity's effect on cogging torque's amplitude. The amplitude decreased on the PMM500 or increased on the PMM1500 with increasing eccentricity.

Axial forces were modelled with 3D models. Axial eccentricity mainly increased axial force's DC component. This increment was not linear but instead started to saturate with higher eccentricities. Axial eccentricity also decreased the radial force as the decreasing axial length decreased the overall magnetic flux density. The results of the created analytical calculation tool compared to the axial force of the PMM500 machine were promising. The overall difference between the force calculated by the analytical tool and the measurements of the whole machine was only 7.37%. The difference was higher when compared to 3D-FEM results. This is due to axial force not increasing linearly with increasing eccentricity, which is the basis for calculation with an analytical model. However, the model could not be compared to other machine types. Thus, more verification is required before the credibility of this model can be summarised.

Keywords: permanent magnet synchronous machines, PMSM, eccentricity, radial eccentricity, radial force, axial eccentricity, axial force, 3D-FEM, modelling.

TIIVISTELMÄ

Hans Porras: Epäkeskeisyydestä aiheutuvat voimat kestomagneettisähkökoneissa
Diplomityö
Tampereen yliopisto
Sähkötekniikan diplomi-insinöörin tutkinto-ohjelma
Toukokuu 2022

Epäkeskeisyydet aiheuttavat voimia ja harmonisia komponentteja sähkökoneissa, minkä seurauksena kone kuluu ja sen käyttöikä lyhenee. Epäkeskeisyydestä aiheutuvien voimien määrittäminen on tärkeää, jotta ne voitaisiin estää tai niiden vaikutusta pienentää. Diplomityö tehtiin Yaskawa Lappeenrannalle, ja sen tavoitteena oli mallintaa erilaisten epäkeskeisyyksien aiheuttamia voimia ja selvittää 3D-FEM mallinnuksen käytännöllisyyttä yrityksen näkökulmasta. Työssä luotiin yksinkertainen analyyttinen malli aksiaalisten voimien arvioimiseksi. Laskentamallia vertailtiin 3D-FEM tuloksiin ja mittauksiin. Tämän opinnäytetyön aikana luodut FEM-mallit olivat ensimmäisiä 3D-malleja, joilla määritettiin sähkömagneettisia ominaisuuksia yrityksen koneissa.

Yaskawalla Lappeenrannalla sähkömagneettiset laskennat tehdään Altair Flux ohjelmalla. Diplomityöhön valittiin kaksi konetyyppiä PMM500 ja PMM1500, joista ensimmäinen edustaa uppomagneettikonetta ja jälkimmäinen pintamagneettikonetta. Koneet mallinnettiin 2D-malleilla ja 3D-malleilla. Koneiden mallit pohjautuvat aitoihin geometrioihin ja materiaalitiedot valittiin Fluxin ja Yaskawan tietokannoista. 3D-mallinnuksen käytännöllisyys rajoittuu kahdesta syystä. Ensimmäiseksi teknisistä rajoituksista johtuen kokonaisia koneita ei voitu täysin mallintaa, joten luodut 3D-mallit sisällyttivät vain osan oikean koneen osapakoista. Toiseksi laskenta-aika kasvaa huomattavasti, minkä seurauksena sähkömagneettisissa tarkasteluissa kestää kauemmin.

Säteittäisestä epäkeskeisyydestä aiheutuvat radiaalivoimat mallinnettiin 2D-FEM laskennalla. Säteittäinen epäkeskeisyys kasvattaa säteittäisvoiman DC-komponenttia lineaarisesti molemmilla koneilla. Säteittäisvoima kasvaa koneen permeanssierosta johtuen niin, että voiman suunta on lyhyimmän ilmavälin suuntaan. Voiman kasvaessa voitiin myös havaita harmonisia värähtelyjä, jotka olivat seurausta kahdesta eri lähteestä. Päävärähtely aiheutuu staattorin urituksen vaikutuksesta, mutta lisäksi epäkeskeisyys aiheuttaa värähtelykomponentteja matalammilla taajuuksilla ja pienemmillä amplitudeilla. Radiaalisen epäkeskeisyyden vaikutusta hammasvääntömomenttiin ei voitu määrittää, koska PMM500 koneella se pieneni, kun taas PMM1500 koneella se kasvoi suhteessa epäkeskeisyyden kasvuun.

Akselin suuntaisesta epäkeskeisyydestä aiheutuvia aksiaalivoimia mallinnettiin 3D-FEM laskennalla. Aksiaalisen epäkeskeisyyden seurauksena aksiaalivoiman DC-komponentti kasvoi. Kasvu ei kuitenkaan ollut lineaarista vaan epäkeskeisyyden kasvaessa alkoi aksiaalivoima tasaantua jotain arvoa kohti. Aksiaalinen epäkeskeisyys vähensi myös säteittäistä voimaa, koska koneen aktiivinen pituus lyheni, mikä puolestaan pienensi kokonaismagneettivuontiheyttä. Työn aikana kehitettiin laskentatyökalu, jolla voitaisiin arvioida aksiaalisiavoimia.

Laskentatyökalu on tehty Yaskawan toiveiden mukaiseksi. Laskentamalli on määritetty epäkeskeisyydestä aiheutuvien geometristen poikkeamien perusteella, mutta se ei perustu aikaisempaan tutkimukseen. Laskentatyökalulla määritetyt voimat ovat kuitenkin huomattavan lähellä mittauksissa saatujen voimien arvoja. Kokonaisero analyyttisen laskentamallin ja mittausten välillä oli vain 7,37 %. Kuitenkin analyyttisen mallin ero 3D-FEM laskennalla saatuihin tuloksiin oli suurempi kuin koko koneen mittauksilla. Analyyttisessä laskentamallissa oletetaan aksiaalivoiman kasvavan lineaarisesti osapakkojen määrän suhteen, mutta FEM-tulosten perusteella tämä ei pidä paikkaansa. Mittausdataa oli vain PMM500 koneelle, joten laskentamallia täytyy vielä verrata muihin tuloksiin tulevaisuudessa.

Avainsanat: kestomagneetti tahtikoneet, PMSM, epäkeskeisyys, radiaalinen epäkeskeisyys, radiaalinen voima, aksiaalinen epäkeskeisyys, aksiaalinen voima, 3D-FEM, mallinnus.

PREFACE

I want to thank everyone who supported me during this thesis. Also, special thanks to Yaskawa Lappeenranta for providing me with this subject, helping me with practicalities, and guiding me through the work. Lastly, I'd like to thank Paavo Rasilo for supervising the project.

Tampere, 20.5.2022

Hans Porras

CONTENTS

ABBREVIATIONS AND SYMBOLS

Abbreviations:

2D	Two-dimensional
3D	Three-dimensional
ARV	Average rectified value
FEM	Finite element method
IPMSM	Internal permanent magnet synchronous machine
PMSM	Permanent magnet synchronous machine
SPMSM	Surface permanent magnet synchronous machine
UMP	Unbalanced magnetic pull

Symbols:

a	Fringing coefficient
a_{ph}	Number of phases
$A_{\Delta z}$	Area of magnet displacement
$\boldsymbol{B}$	Magnetic flux density
B_{g}	Air gap magnetic flux density's magnitude
$B_{\mathrm{g}}^{\mathrm{a}}$	Magnetic flux density created by armature
B_{g}^{m}	Magnetic flux density
$B_{\mathrm{g}n}^{m}$	Fourier's coefficients of flux density
B_{r}	Remanence magnetic field
$\boldsymbol{D}$	Electric flux density
D_{ri}	Rotor's diameter
$\boldsymbol{E}$	Magnetic field
E_0	Phase voltage
f	Main supply frequency
f_{mm}	Magnetomotive force
$f_{\mathrm{mm}}^{\mathrm{a}}$	Magnetomotive force created by armature
F_1	Force component representing UMP's DC component
F_4	Force component representing UMP's vibrations
F_{rad}	Normal force
F_{x}	Normal force's component in x-direction
F_{y}	Normal force's component in y-direction
F_{z}	Magnetic force in z-direction
g	Physical air gap width
g_0	Physical air gap during concentric operation condition
g_{avg}	Average air gap length
$g_{\mathrm{oh,min/max}}$	Furthest point of magnet, which is not under stator slot
h_{m}	Height of a magnet
$\boldsymbol{H}$	Magnetic field strength
I_{m0}	Phase current
$\boldsymbol{J}$	Current density
L	Effective length of the rotor after displacement
L_0	Rotor length
m	Frequency of permeance variation due to stator slotting
n_{r}	Harmonic order of pulsating stress due to armature reaction
p	The number of pole pairs
Q_{s}	Number of stator slots
R	Rotor radius
S	Surface area
ss	Number of stator stacks
t	Time

T_{e}	Electromagnetic torque
t_{p}	Periodicity of the machine
v_{e}	Harmonic order created by radial eccentricity
V	Volume of the air gap
w_{cd}	Cooling duct width
w_{oh}	Width of the part of magnet, which is not under stator slot
w_{PM}	Permanent magnet width
w_{ss}	Stator slot width
W	Energy stored in the air gap
x	Air gap width of a part of a magnet, which is not under stator slot
x_{avg}	Average air gap width of a part of a permanent magnet, which is not under stator slot
$x_{\mathrm{avg,min/max}}$	Average air gap length of the part of magnet, which is not under stator slot
α	Angle between closest point of permanent magnet and stator slot's edge
β	Maximum angle of θ
β_{m}	Magnet pitch
δ_{s}	Relative eccentricity
Δz	Axial displacement
θ	Calculation position around rotor
θ_{ss}	Angle between x and g_0
Θ	Slot's position in angles
λ_0	Mean value of permeance variation
λ_{e}	Relative permeance due to eccentricity
$\lambda_{\mathrm{e}\mu}$	Fourier's coefficients for permeance due to eccentricity
λ_{n}	Fourier's coefficients for permeance due to stator slotting
λ_{r}	Relative permeance
Λ	Permeance
Λ_0	Permeance during concentric operation condition
μ_0	Permeability of free space
μ_{rm}	Relative permeability of the magnet
ρ	Electric charge density
σ_{Frad}	Normal stress
σ_{Ftan}	Shear stress
$\sigma_{\mathrm{pole,rad}}$	Normal stress over pole
$\sigma_{\mathrm{rs,rad}}$	Normal stress over rotor stack
φ	Magnet's initial position
Φ	Magnetic flux
ψ	Virtual displacement
ω_{m}	Mechanical speed

1. INTRODUCTION

Electrical machines are used widely in multiple different applications. They can produce power for electrical networks or consume power in automotive and marine applications. Permanent magnet synchronous machines (PMSM) have high power conversion efficiency, power density, and simple design, so they can be used in many applications [1–3]. Constant development is required to increase the efficiency, operate the machines safely, and extend the lifetime of these machines. Different models and operating conditions can be researched without building a prototype by electromagnetic modelling. The finite element method (FEM) is the primary way to calculate the electromagnetic properties of machines due to its efficiency, accuracy, and ability to calculate non-linearities [1,4,5].

Electrical machines may experience eccentric operation conditions due to manufacturing tolerances, misalignments during assembly, and wear during their lifetime [6,7]. The phenomena happening due to these conditions can be modelled. This thesis focuses on eccentric operation conditions, which can be split into multiple categories. The primary split is the direction of the eccentricity. If the rotor is offset from the stator in the radial direction, the eccentricity is called radial eccentricity, whereas the axial eccentricity refers to the offset in the axial direction. These eccentricity types can exist simultaneously, which results in even more complicated phenomena [7]. Furthermore, eccentricity may be static, dynamic, or mixed depending on the minimum air gap's position relative to time. This thesis is limited to covering static radial and axial eccentricities. The radial static eccentricity may be caused by an asymmetric stator, radial misalignment of the rotor, or bearing wear, as all create conditions where the angle of minimum air gap does not change [6]. On the other hand, the axial eccentricity can be induced by axial misalignment of the rotor or external forces offsetting the rotor [7].

Eccentricities cause a variety of problems for the machine's operation during the lifetime, but the main effect for both resultant forces is the same for both eccentricities. The higher the eccentricity, the higher the static force is created in the same axis as the eccentricity. [7] Additionally, the eccentricity will induce sinusoidal components into the forces, and the amplitudes of existing harmonic components grow [4,7]. Depending on the severity of the fault, eccentricity may break the machine or cause significant wear for the machine over its lifetime. It increases the operational and maintenance costs of the machine. These

force components affect all the infrastructure around electrical machines through the casing and shaft [8]. Both radial and axial forces are transferred through the shaft to bearings, which are built to withstand radial forces, like the gravity of the machine. Still, axial forces induced by axial eccentricity may break them. Furthermore, harmonics induced due to eccentricity generate vibrations, which may result in audible sound and endanger the expected lifetime of the system.

The aim of this thesis is to model the electromagnetic properties of a machine in eccentric operating conditions and to review if three-dimensional (3D) FEM modelling could be integrated to be included in the electrical modelling process. This is realised by 3D-modelling of the machines and by creating a simple analytical calculation tool, which can approximate the axial forces based on machines' properties. These results can be used to choose optimal bearings for the machine and to calculate construction tools for the machines. Radial eccentricity is a well-researched topic, but this thesis also focuses on axial eccentricity and the challenges it may bring for assembling and operating the machine in specific conditions. An analytical model is created for the axial eccentricity, which can be used to approximate the force without exact FEM modelling. The results are based on previous studies and models generated during the project.

This thesis includes a literature review and FEM-modelling of two PMSMs. Chapters 2 to 4 are based on a literature review, chapter 5 is based on methods to simulate or measure the forces, and in chapter 6, the results obtained with the models are reviewed. Chapter 2 covers the PMSM structure and focuses on the machine's parts, which influence the forces. These influences are further divided between parameters of machine parts to depict which parameters impact the force in which way. The third chapter focuses on electromagnetic forces in electrical machines. The chapter starts from the basis of electromagnetic calculations and further covers the calculations used in FEM software and analytical calculations, which depict the sources of force components. The fourth chapter covers unbalanced magnetic pulls and the impacts on different force components. The fifth chapter covers the modelling done in this thesis. The sixth chapter contains a comparison of the results obtained with all models. The seventh chapter concludes the findings of this research.

2. MACHINE MODEL

The main components of electrical machines are rotor and stator. The rotor creates a rotating magnetic field, which induces currents to conductors located on the stator side. The operation of an electrical machine is based on electromagnetic forces, which are created by magnetic flux. The following subchapters consist of different parts of the electrical machine that affect the air gap flux density and thus impact the forces by affecting their amplitude, harmonic content, or the combination of the two. [9]

2.1 Permanent magnets

Permanent magnets are used in PMSMs to excite the machine. A permanent magnet's flux density waves are trapezoidal by nature as the magnet's shape dictates the created flux. The voltage induced on stator winding can still be nearly sinusoidal with proper design despite the trapezoidal flux shape. Permanent magnets are positioned on the rotor, and flux waves rotate when the rotor is rotated. This creates the main component of the changing magnetic field, which induces current into the windings on the stator side and produces power when the machine is operated. [9]

The attributes of the magnetic material vary between different magnet types. The most common characteristics considered when choosing a permanent magnet material are coercivity, remanence flux density, and price [9]. Coercivity determines how high external magnetic field strength is required to reduce the magnetic flux density to zero. In practice, coercivity is selected based on a short circuit event, which causes a demagnetising magnetomotive force component demagnetising the magnets. Remanence flux density instead informs how high flux density is left in the material after it has been magnetised in an external magnetic field and taken out of it. Magnetic materials with higher remanence flux densities create higher air gap flux densities. Thus, less magnetic material is required. Remanence flux density decreases in proportion to the operating temperature, and the point when the magnet demagnetises due to too high temperature is called Curie temperature. Demagnetisation poses a significant risk in the machine even though losses on the rotor side of a PMSM are negligible. [9] If permanent magnets reach Curie temperature, the magnets lose their magnetism entirely, and the only way to get it back is to remagnetise the magnets. However, Curie temperature with modern magnets is so high that it is practi-

cally unreachable unless there is a severe fault. Price determines which magnet with the correct technical statistics is selected.

In addition to the magnet remanence, the permanent magnet thickness is used to control the air gaps flux density to an appropriate level. Thicker magnets create higher flux densities and vice versa. [9]

Finally, the permanent magnet's mounting type significantly affects the created flux wave. Permanent magnets can be placed on the rotor surface or within the machine. Machines which have surface magnets is called the surface magnet rotor, or surface magnet permanent magnet synchronous machine (SPMSM). Machines which have embedded magnets are called the embedded magnet rotor or internal permanent magnet synchronous machine (IPMSM). Figure 1 shows examples of both machine types.

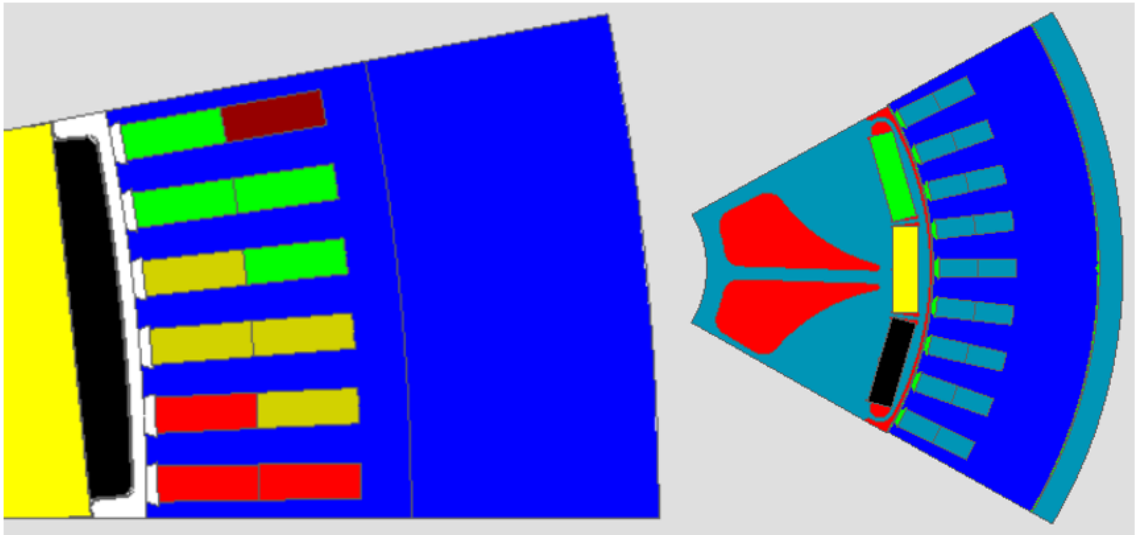

Figure 1: Examples of surface mounted and embedded mounted permanent magnets.

On the left side of Figure 1. is the surface mounted rotor type and embedded magnet type machine on the right side. Location affects the machine's properties significantly. This also means that the rotational speed is capped due to magnets experiencing centrifugal stresses, which may break or loosen them. Embedded magnets do not have the same problem as they are well supported in their pockets. Magnets in embedded magnet machines can be structured to make the magnetic flux density more sinusoidal, but the magnets on the surface must follow the surface structure. Alternatively, magnets on both machines can be skewed to reduce the cogging torque created by trapezoidal flux densities. [9] Cogging torque is the torque component which overcomes the magnetic force between the magnets on the rotor and the stator teeth.

Skewing means offsetting the magnets or stator slots tangentially from each other in the axial direction. Skewing the magnets on the rotor side is easier on PMSM, and it is preferred. The main benefit of skewing the magnets is to reduce harmonics in the air gap flux density. Reducing harmonic components will decrease tangential vibrations in the machine, make the machine run smoother, and reduce noise. Skewing is done in steps. [9] An example of skewing is given in Figure 2.

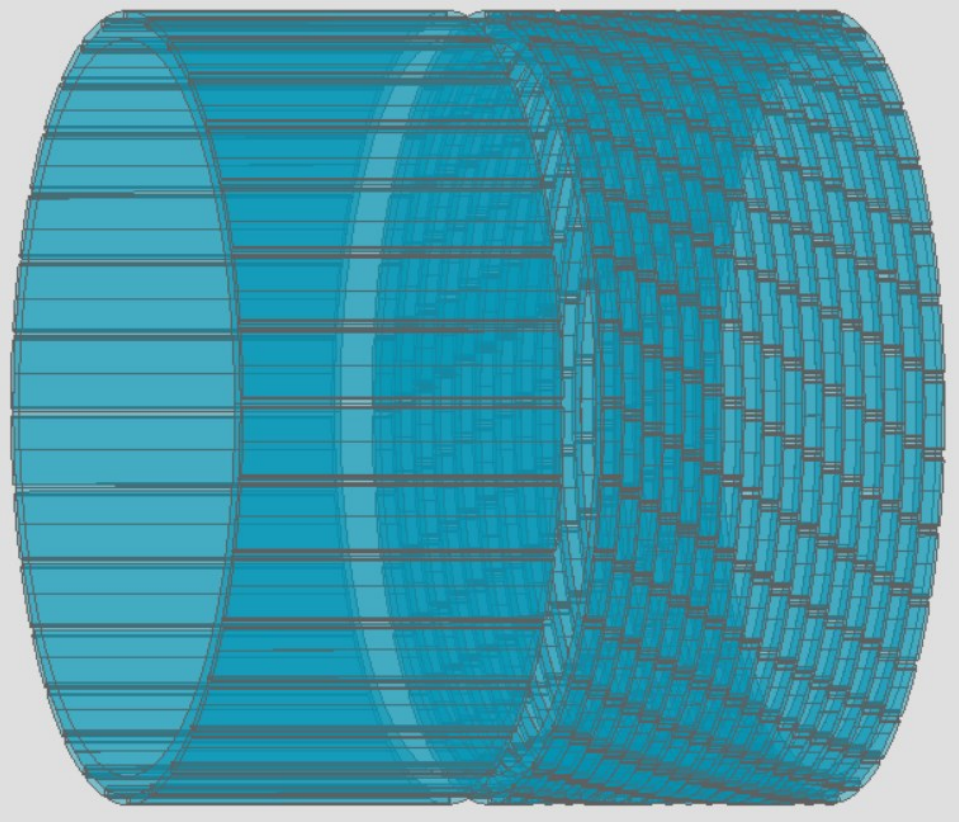

Figure 2: Example of magnet skewing.

Figure 2 shows how skewing is reduced to a finite number of steps. The number of steps can be calculated by dividing machine width by magnet width. Step skewing can be further controlled with 2 different components:

- Skewing angle
- Number of tangential positions

Both components affect the magnetic flux density separately. But the basic principle of skewing stays the same. As the magnets are offset tangentially, the back-emf becomes more sinusoidal. This also reduces the maximum flux density a bit. Cogging torque is generated due to magnet edges going past slot edges, so by dividing the edges into multiple positions amplitude of cogging torque lowers. [9]

Skewing angle is determined as the angle of the tangential shift between magnets. Skewing angle affects which harmonics are eliminated from the system. Research by Wang et al. [2] focuses on skewing's effects on radial vibrations. As radial forces are the largest in electrical machines, they can be used to reduce noise significantly. Their study concluded that smaller skew angles decrease higher harmonic components of radial force, and as the skew angle is increased, lower harmonics decrease [2]. Specific skewing angles can eliminate specific time-harmonic. Lower harmonic components have higher amplitude, so the increasing angle will continuously lessen the vibrations. Ultimately, this will reduce torque, so the skewing angle must be optimised based on electromagnetic operation and the vibrations. Ali et al. [10] optimised skewing angle based on cogging torque. They found that the cogging torque is at a minimum when the skewing angle is equal to the stator slot pitch due to skewing effectively eliminating the slot harmonics. A smoother torque curve will result in more sinusoidal currents and voltages and reduce overall stresses.

The number of tangential positions affects the forces by dividing the flux density more evenly in the air gap. Due to the stepping nature of the skewing, some harmonics cannot be reduced from flux density. Wang et al. found out that increasing the number of steps will increase the frequencies of harmonic components, which are not affected by the skew [2]. This means that effectively fewer steps will result in worse vibrations, but increasing the number of steps will not increase the vibrations infinitely as the amplitudes of higher harmonics decrease rapidly [2]. Xing et al. have researched the effect of increasing the number of steps to cogging torque [11]. They found that increasing the number of tangential positions of magnets will decrease the cogging torque. This reduction becomes small after 4 tangential positions in their machine. This means that the number of magnet posi-

tions should not be increased too much. It may overcomplicate the machine's structure which results in higher building costs.

2.2 Air gap

The air gap is the gap between stator and rotor bodies. It is significant for mechanical operation and impacts the magnetic flux density. Most critical electromagnetic parameters are calculated inside the air gap or on its edge. Air's reluctance value is much higher than steel's, which means that magneto-motive force (MMF) over the air gap is high. Thus, magnetic energy is mainly consumed within the air gap, resulting in forces being generated in the air gap. The main controllable parameter is air gap width. [9]

The air gap width is often decided with techno-economic analysis, and it varies between different machine types. The baseline is that a smaller air gap requires less magnetic materials to achieve the same magnetic flux density as a wider air gap but comes with the cost of increasing leakage inductance and rotor surface losses due to eddy currents. The air gap must be designed so that the rotor and stator cannot contact due to tolerances in manufacturing or minor faults. Wider air gaps are better during eccentric operation situations as the relative change is smaller. Hence, the unbalanced magnetic pull is smaller compared to machines with smaller air gaps but similar specifications. [9]

There are two types of PMSMs, so the air gaps between them differ a lot. Permanent magnets have similar permeability to air, and thus the magnetic air gap width on surface mounted machines is a combination of the physical air gap and magnet thickness. Variation of air gap width's effect on air gap's flux density is smaller on SPMSM than on IPMSM, according to research by Zhao et al. [12].

The air gap's width is uniform with no variations in a theoretical situation, and the basic analytical models are based on this approximation. In practice, air gap width varies periodically due to stator and rotor slots. Rotor slots do not exist in PMSMs, but the stator slots influence magnetic air gap width. [4]

2.3 Stator slots

Stator slots are the slots in the stator body that house the stator windings. These slots vary from machine to machine, with different shapes, sizes, and the number of slots. Stator slots affect the magnetic flux density by increasing the air gap width. This creates a dip in the flux density, which is proportional to the slot's dimensions. The main dimensions affecting the magnetic flux density are slot width, slot depth, and the number of slots. Slot wedge al-

so impacts the magnetic flux density, but both machines are modelled without slot wedges. [9]

There have been multiple ways to calculate stator slots' effects on flux density. Calculations have been done traditionally via simplifying machine geometry. One of the oldest calculation methods is Carter's factor, provided by F. W. Carter already in 1901 [9]. Newer methods, including less simplifying and generating more exact results, were invented later. One of these methods is the relative complex permeance method. This method considers slot effects by calculating relative permeance, which includes harmonics created by stator slots [8]. According to the method, the slots create forces in a tangential direction, thus affecting the torque [13]. The radial force is affected by combinations of effects of stator slots and armature reaction or stator slotting [8]. Stator slots create the main vibrational component found in electrical machines. As the rotor pole passes the edge of the tooth, a magnetic attraction force is generated, which tries to lock the rotor into that position.

Stator windings are coils within the stator slots. Rotating magnetic fields generated by permanent magnets induce electromagnetic force (emf) into stator windings. There are many possible stator winding types utilised to create the optimal waveform for different machine types. The most common divisions between winding types are:

- Distributed or concentrated
- Integral or fractional
- Single layer or multilayer
- Short-pitched or full-pitched

The windings are usually polyphase distributed windings in PMSMs. Polyphase means that the windings in coils are divided into multiple phases, most commonly three, as a three-phase network is mainly used. Distributed winding means that the windings are spatially separated across the machine, which means that the coil is not formed around a single tooth on the stator side. Instead, it is distributed to multiple slots, slightly reducing the generated emf and improving the waveform by making it more sinusoidal. Integral or fractional windings can be calculated by dividing the number of slots by the number of phases and poles. If the result is a fraction, the winding is fractional. Fractional slot winding affects the operation of the machine by giving better freedom with the number of slots, multiple short-pitching options, and the possibility of removing some harmonics. The drawback is that fractional winding creates subharmonics in certain conditions. Both machines considered in this thesis are integral slot machines. The stator slots are not divided into

parts in single layer machines, but in multilayer slots, the slot is divided into parts. This allows for short pitching of the windings. Short pitching means shifting ends of the coils by a multiple of a slot pitch, and it can be used to alter the harmonic content of the flux density. [9]

2.4 Cooling channels

Cooling channels are air gaps between the stator and rotor discs in the axial direction. They are mainly used to lower the temperature in the machine during operation. Operation temperature increases due to losses in machines generating heat. Ultimately temperature rise may result in demagnetisation of magnets. The main losses contributing to heat generation in electrical machines are so-called iron losses in steel laminations and so-called copper losses in coils due to Ohm's law. Also, mechanical losses (turbulence, friction) in the air gap area can be significant, especially at higher speeds. Copper losses can be further divided into the stator and the rotor side losses. There are no copper losses on the rotor side in permanent magnet machines as the windings are replaced with magnets. This reduces the heat generation in the rotor significantly. As the magnetic flux in the rotor yoke has only a DC component, the iron losses are close to 0. For this reason, the rotor yoke on SPMSM machines can be a continuous cylinder, which simplifies rotor structure significantly. Embedded magnet machines benefit from cooling channels on the rotor side as magnets can be positioned more easily. [9]

Kim et al. suggest in their study that cooling channels alter the distribution of axial force[14]. Different cooling channel structures affect the axial force induced by axial eccentricity. There may be multiple magnetic neutral positions, which would mean that the rotor could lock to a position offset from the middle plane. Higher axial forces would be beneficial in most applications because the rotor is centred better, but if the pull is going to affect the bearings, smaller forces are a better option. The study conducted by Kim et al. covers only a couple of cooling channel options and only with an axial two-dimensional (2D)-FEM [14]. Optimising cooling channels regarding axial forces could be a further study.

3. ELECTROMAGNETIC FORCES IN ELECTRICAL MACHINE

Electromagnetism is based on Maxwell's equations. Maxwell's equations are

$$\nabla \times \boldsymbol{E} = -\frac{\partial \boldsymbol{B}}{\partial t}, \tag{1}$$

$$\nabla \times \boldsymbol{H} = \boldsymbol{J} + \frac{\partial \boldsymbol{D}}{\partial t}, \tag{2}$$

$$\nabla \cdot \boldsymbol{D} = \rho, \tag{3}$$

$$\nabla \cdot \boldsymbol{B} = 0. \tag{4}$$

The first of the laws is called the curl relation of an electric field, the second is called the curl relation of the magnetic field, the third divergence equation of electric flux, and the last one is the divergence equation of magnetic flux density. Variables in the formulas are electric field strength $\boldsymbol{E}$, magnetic flux density $\boldsymbol{B}$, magnetic field strength $\boldsymbol{H}$, electric flux density $\boldsymbol{D}$, current density $\boldsymbol{J}$, and electric charge density ρ .In chapter 3 the magnetic forces are covered thoroughly, but magnetic flux density together with magnetic field strength are one of the most important components in determining them. For this reason, (1),(2), and (4) are covered more thoroughly in this chapter in their integral forms. [9]

The first of the laws is also called Faraday's induction law. It can be expressed as an integral form

$$\oint_l \boldsymbol{E} \cdot \mathrm{d}l = -\frac{d}{dt}\int_S \boldsymbol{B} \cdot \mathrm{d}\boldsymbol{S} = -\frac{d\Phi}{dt}, \tag{5}$$

in which Φ is magnetic flux. It states that the negative line integral of electric field strength following a closed path is equal to changing magnetic flux going through an open surface $\boldsymbol{S}$. This law and Ampere's law can be used to calculate induced voltages and eddy current losses in an electrical machine. [9]

The second law can be also called Ampere's law. The integral form of the Ampere's law is

$$\oint_l \boldsymbol{H} \cdot \mathrm{d}l = \int_S \boldsymbol{J} \cdot \mathrm{d}\boldsymbol{S} + \frac{d}{dt}\int_S \boldsymbol{D} \cdot \mathrm{d}\boldsymbol{S}, \tag{6}$$

which states that the integral of the magnetic field strength along the closed path is equal to the current going through a surface and the change of electric flux. It can be used to approximate magnetic voltages and required current linkage in the electrical machine. Current linkage is the sum of currents flowing in the windings. [9]

Equation (7) depicts Gauss's law for magnetic fields. Gauss's law's integral form is

$$\oint_S \boldsymbol{B} \cdot \mathrm{d}\boldsymbol{S} = 0, \tag{7}$$

in which $\boldsymbol{S}$ is a closed surface. In this form, the law states that the integral of magnetic flux density over a closed surface is 0. This means that magnetic flux does not have a starting or ending point but instead flows in an endless loop. For example, the main flux flows within the magnetic circuit in electrical machines. [9]

Maxwell's equations are the basis for electromagnetic calculations, but solving them analytically may be impossible as the calculations depend on the machine's geometry, material properties, and time dependency. This thesis further looks at analytical equations, which include approximations and assumptions. Maxwell's equations are used within the FEM calculation software.

3.1 Maxwell's stress theory

Magnetic field strength between objects in free space creates stresses on the object's surface. Maxwell's stress theory can approximate these stresses and the forces that the stresses make. [9] Maxwell's stress theory is commonly used in analytical calculations as a basis to calculate radial and tangential force components [8,15,16].

The theory proceeds from Faraday's statement, which says that stress occurs on the flux lines. Commonly, Maxwell's stress theory is simplified to be calculated with traction vectors instead of the tensors. Traction vectors have the same units as stress but are vectors instead of a tensor. The traction vector, which affects a cylindrical surface in the machine's air gap, can be split into two components. [9]

The tangential component is the shear stress, which creates the spinning motion for the rotor, and it can be approximated by

$$\sigma_{\mathrm{Ftan}} = \mu_0 H_{\mathrm{rad}} H_{\mathrm{tan}}, \tag{8}$$

in which, μ_0 is the permeability of free space and H is the magnetic field strength between objects in free space and subscripts rad and tan denote the radial and tangential direc-

tions, respectively. The radial component of the magnetic traction is normal stress, which can be calculated by

$$\sigma_{\mathrm{Frad}} = \frac{1}{2}\mu_0(H_{\mathrm{rad}}^2 - H_{\mathrm{tan}}^2). \quad (9)$$

Both tractions create force vectors, but σ_{Ftan} is more significant for the basic operation of the machine as it creates the torque. [9] On the other hand, normal stresses are higher, but radial forces created by the traction cancel themselves out during normal operating conditions. When there is a radially eccentric operation condition, resultant radial forces are much larger than in the case of torque, which can be seen from the second power of magnetic field strength.

3.2 Magnetic flux density

Magnetic flux density is composed of magnetomotive forces of rotor and stator and permeance of the machine. Its value differs around the machine, but as it is symmetrical across all the poles, flux density waves repeat periodically.

Magnetic flux density can be written as

$$B(\theta, t) = f_{\mathrm{mm}}(\theta, t)\Lambda(\theta), \quad (10)$$

in which B is magnetic flux density, f_{mm} is the magnetomotive force vector, and Λ is permeance. Based on (10) effects of permanent magnets, conductors on the stator side and by permeance varying components are evaluated. Analytical expressions of magnetic flux densities created by permanent magnets and armature reactions are covered for slotless machines. Machine slots are going to be considered with relative permeance. [3]

As discussed in the previous chapter, magnetic flux densities generate magnetic traction on surfaces. This stress oscillates due to variations in magnetic flux density. The effects of vibration of the given magnetic flux density component are evaluated on the rotor reference frame. On the rotor side, these variations are generated by the armature reaction of stator windings or effects of the stator slots, as the flux created by permanent magnets is constant in reference to the rotor surface. [4]

3.2.1 Magnetic flux density created by the permanent magnets

The primary excitation method is permanent magnets. Magnetic flux density's magnitude created by permanent magnets can be calculated with

$$B_{\mathrm{g}} = \frac{B_{\mathrm{r}}}{1 + \frac{g \cdot \mu_{\mathrm{rm}}}{h_{\mathrm{m}}}}, \tag{11}$$

in which B_{g} is the magnitude of air gap magnetic flux density, B_{r} is the remanence of the magnetic field, h_{m} is the height of the magnet, g is air gap length from top of the magnet to stator, μ_{rm} is the relative permeance of the selected magnet type [4]. Magnets of an electrical machine are spatially distributed based on their locations, and as the rotor rotates the spatial distribution changes. Thus, magnetic flux density distribution is

$$B_{\mathrm{g}}^{m}(t,\theta) = \sum_{n=1}^{+\infty} 2 \cdot B_{\mathrm{g}n}^{m} \cos\big(pn(\varphi + \omega_{\mathrm{m}} t - \theta)\big), \tag{12}$$

in which $B_{\mathrm{g}n}^{\mathrm{m}}$ are the coefficients of the Fourier series of flux density, p is the number of pole pairs in the rotor, φ is the initial position of the magnet, ω_{m} is mechanical speed and θ is the calculation position around the rotor. Coefficients can be calculated with

$$B_{\mathrm{g}n}^{\mathrm{m}} = \frac{B_{\mathrm{g}}}{n\pi} \cdot (1 - \cos(n\pi)) \cdot \sin\left(np \cdot \frac{\beta_{\mathrm{m}}}{2}\right) \cdot \frac{2}{1 + (a \cdot n \cdot p)^2}, \tag{13}$$

in which β_{m} is the magnet pitch and a is a fringing coefficient [4]. The magnetic flux density of a permanent magnet is not purely square pulse, which is why the fringing coefficient is used to adjust the waveform to be more realistic. The fringing coefficient can be approximated with

$$a = \frac{\sqrt{g \cdot \left(g + \frac{h_{\mathrm{m}}}{\mu_{\mathrm{rm}}}\right)}}{D_{\mathrm{ri}} + 2h_{\mathrm{m}} + g}, \tag{14}$$

in which D_{ri} is the inner diameter of the rotor. From (13) can be seen that with appropriate magnet pitch, some harmonics from force can be reduced or diminished. [4]

3.2.2 Magnetic flux density created by the armature reaction

Armature reaction creates a magnetic flux density component. This component can be calculated with

$$B_{\mathrm{g}}^{\mathrm{a}}(t,\theta) = \mu_0 \cdot \frac{f_{\mathrm{mm}}^{\mathrm{a}}(t,\theta)}{g}, \tag{15}$$

in which $B_{\mathrm{g}}^{\mathrm{a}}(t,\theta)$ is magnetic flux density of the armature reaction in the air gap, and $f_{\mathrm{mm}}^{\mathrm{a}}(t,\theta)$ is the magnetomotive force created by the coils. The magnetomotive force of the armature reaction of a single-phase can be calculated based on the distribution of the conductors and the phase current. By summing these magnetomotive force components,

overall force is obtained, which can be placed into (15). Armature reaction does not generate magnetomotive force harmonics, which orders are multiples of 3. [4]

The magnetic flux created by armature reaction can be split into principal and spatial components. The principal component is synchronous to the magnetic flux produced by the magnets, so it propagates with the same velocity and direction. The rest of the components propagate at different velocities and directions. The pulsation of a harmonic is based on the difference between the velocities of the rotor speed and the propagating pulse. Harmonic orders can be evaluated by

$$n_{\mathrm{r}} = \left(s\frac{p}{t_{\mathrm{p}}} - n\right)\frac{t_{\mathrm{p}}}{p}, n \in 1{,}5{,}7{,}11{,}\ldots\ , s = \pm 1, \tag{16}$$

in which s is defining the propagation direction and t_{p} is the periodicity of the machine. Periodicity is the greatest common divisor of the number of stator slots (Q_{s}) and pole pairs (p). On integer machines, the $\frac{p}{t_{\mathrm{p}}}$ relationship always equals one, which means that the harmonic orders can be simplified to form

$$n_{\mathrm{r}} = s - n. \tag{17}$$

It can be deduced that the harmonic content of magnetic stress includes harmonics with orders of multiplies ± 6 due to armature reaction on stator windings. [4]

3.2.3 Change in magnetic flux density due to permeance variations

The forementioned equations are calculations for a slotless permanent magnet machine. Permanent magnet machine's slots are influenced by air gap permeance. Permeance is the inverse of reluctance, and it can be calculated with

$$\Lambda(\theta) = \frac{\mu_0}{g(\theta)}, \tag{18}$$

in which $g(\theta)$ is the radial length of the air gap. Within the slotless machine, permeance during a normal operating condition is a constant as $g(\theta)$ does not change so that the permeance can be denoted with Λ_0. In practice, the permeance varies because of the stator slots or eccentricities in the radial direction. Axial eccentricities do not affect the permeance as it does not affect the radial length of the machine. [7]

Basically, Λ_0 would be the permeance of an ideal machine, and g_0 would be the air gap length of an ideal slotless machine. Therefore, the relative permeance of the machine can be denoted with

$$\lambda_{\mathrm{r}}(\theta) = \frac{\Lambda(\theta)}{\Lambda_0} = \frac{g_0}{g(\theta)}, \tag{19}$$

in which $\lambda_{\mathrm{r}}(\theta)$ is the relative permeance and $\Lambda(\theta)$ and $g(\theta)$ are permeance and air gap length respect to angle. Relative permeance is dimensionless, and thus the actual magnetic flux density components in a slotted machine is calculated by multiplying the magnetic flux densities with relative permeance. [17]

The relative permeance of a slotted machine can be approximated with

$$\lambda_{\mathrm{r}}(\theta) = \lambda_0 + \sum_{n=1}^{+\infty} \lambda_n \cos\left(Q_{\mathrm{s}} n(\Theta - \theta)\right), \tag{20}$$

in which λ_0 is the mean value of permeance variation, λ_n are Fourier's coefficients, and Θ is the slot's position from the x-axis in angles. [4]

The magnetic flux density crossing the rotor's surface varies due to stator slots. The frequency of this permeance variation is

$$m = n\frac{Q_{\mathrm{s}}}{p}, n \in \mathbb{N}, \tag{21}$$

in which m is the frequency of the variation in flux density. From (21) can be seen that by modifying the $\frac{Q_{\mathrm{s}}}{p}$ ratio, the frequencies of these harmonics can be altered. As n can be any positive integer, harmonic spectrum considering forces includes all multiples of $\frac{Q_{\mathrm{s}}}{p}$. [4]

3.3 Forces

The main force components generated in electrical machines are radial, tangential, and axial forces. The radial force is always present due to magnets pulling themselves towards the stator and is the largest force component inside electrical machines. The sum of these forces over the machine is usually close to zero as the magnets are placed evenly on the machine and other magnets counter the pull created by one magnet. Tangential force is the force that rotates the rotor. Axial force may be induced during start-ups, faulted, or bad operation situations in traditional electric machines. Some machines may constrict the movement of the rotor in the axial direction. Thus, if wrongly positioned, the axial force may create constant wear for bearings throughout the machine's lifetime.

3.3.1 Radial force

Maxwell's stress theory was covered in subchapter 3.1. It states that the stress created by magnetic field strength between objects in free space creates stress on the surfaces of these objects. Stress measures a force over an area. Therefore, we can calculate radial force by taking radial magnetic traction and multiplying it by the cross-sectional area of the air gap. This will result in

$$F_{\mathrm{rad}} = \sigma_{\mathrm{Frad}} \cdot S_{\mathrm{ag}}, \tag{22}$$

in which S_{ag} is the area of the air gap [9]. The area of the air gap is a cylindrical area around the rotor. As the radial magnetic flux density is much larger than the tangential flux density, σ_{Fn} is simplified to include only the radial component. Additionally, the radial force can be calculated per unit area. With modifications (22) changes to form

$$F_{\mathrm{rad}}(t) = \frac{B_{\mathrm{n}}^2(\theta, t)}{2\mu_0} \cdot S_{\mathrm{ag}}(\theta), \tag{23}$$

in which $F_{\mathrm{rad}}(t)$ is the radial force, with respect to angle and time. [9] From (23) can be deduced that the radial force's harmonic components depend solely on the magnetic flux densities' harmonic components.

Radial force can be calculated over the whole machine, or the other common way to calculate it is by splitting it into x- and y-direction components [7]. Radial forces x- and y-components can be calculated with

$$\begin{cases} F_{\mathrm{x}}(t) = L_0 R \int_0^{2\pi} F_{\mathrm{n}}(\theta, t) \cos(\theta)\, d(\theta) \\ F_{\mathrm{y}}(t) = L_0 R \int_0^{2\pi} F_{\mathrm{n}}(\theta, t) \sin(\theta)\, d(\theta) \end{cases}, \tag{24}$$

in which L_0 is the length of the rotor and R is the radius of the rotor. Theoretically, both components should be close to 0 during normal operation of the machine, and the eccentric operation can be seen as an increase on either or both components. In practice, there are constantly small vibrations in the machine due to the slotting effect which it must be able to withstand. [7]

Due to harmonics in the magnetic flux density, multiple radial force waves are rotating around the machine. These force waves bend the stator core and cause deformation. Bending is higher on lower order radial force waves with high amplitudes, and these also contribute most to the vibration [16,18]. Deforming can be approximated by the force wave's power and amplitude, where it is inversely proportional to the former and proportional to

the latter [16]. The DC component does not induce vibrations but will increase the wear on the bearings [7].

3.3.2 Tangential force

Tangential force is the most influential force in electrical machines as it determines the power generation capability of the machine. Due to this, there are multiple studies regarding how to calculate it. FEM can calculate torque by many methods, for example, Maxwell's stress tensor, Coulomb's, or Arkkio's method [9,15]. In this thesis, torques are calculated with a method based on a virtual work [19]. Additionally, an analytical method based on Coulomb's virtual work method is further analysed so eccentricities effects on torque can be analysed.

Coulomb's virtual work method calculates the energy stored in the air gap and approximates torque by displacement of the force. If losses are ignored, the air-gap magnetic energy is written as

$$W(t) = \int_V \frac{[B(\theta, t)]^2}{2\mu_0} dV, \tag{25}$$

in which W is the magnetic energy and V is the volume of the air gap. Derivative of (25) is equal to torque as a function of virtual displacement, which can be written as

$$T_e(t) = p \frac{\partial W(t)}{\partial \psi(t)}, \tag{26}$$

in which ψ is virtual displacement, with respect to the time. [15] The torque is close to zero when there is no load. Stator slots generate cogging torque, which can be seen as a ripple on the torque curve. In the ideal case, the fundamental component of the cogging torque is the lowest common multiple of the number of slots and the number of poles. [20]

3.3.3 Axial force

The axial force was studied already in 1953 by C.E. Bradford and R. G. Rhudy [21]. Their research was based on a conducting paper model, and they used it to deduct axial force induced by an axial eccentricity. But since then, there has not been much research regarding axial forces, and few studies use the model created by Bradford and Rhudy as a basis [7,22]. In recent years new applications like skewed stator winding have sparked an interest in studying and minimising the generated axial force [23,24]. Still, even then, the overall research interest has been negligible due to the diminishing nature of the force.

The axial force is generated either by an axial air gap or skew of the machine [21,25]. Magnetic force in the axial direction increases with larger eccentricities, but studies imply that the force saturates at some value [22]. Axial force opposes the movement of the rotor, and in a concentric situation with no skewing, the force is 0 [22]. For this reason, if the rotor can move in the axial direction, it will centre itself during operation, and the force diminishes. The axial force is based on the reluctance force generated in the air gap, and it varies based on the air gap flux density [14]. The axial force is higher with higher air gap flux densities like the other forces. Overall the axial force should be smaller than the radial force as the leakage magnetic field produces it and not the main magnetic field [7]. Skewing may induce axial force, but studies show that sinusoidal PM shape can be used to diminish the axial force [25].

4. UNBALANCED MAGNETIC PULL

Unbalanced magnetic pull (UMP) means that the rotor of the electrical machine is experiencing a force that is not balanced by counterforce to the other direction. UMP can be induced in any direction radially, axially, and tangentially. Tangential UMP rotates the machine, but the UMPs in the radial or axial directions should be negated. The main cause of these types of UMPs is eccentricities in machines. Eccentricities covered in this thesis are static radial and static axial eccentricities.

4.1 Radial static eccentricity

There are always radial forces in electrical machines, but the sum of radial force vectors is 0 during the normal operation of the machine as they cancel each other out. Radial static eccentricity is an operating situation where the rotor's axis is misaligned from the stator's axis. The air gap is smaller on one side of the machine than on the other side. The radially eccentric operation condition changes the magnetic flux density distribution and thus the created forces. Decreasing the air gap decreases the reluctance value, which means that the magnetic flux density will increase on the side of the machine, which has a smaller air gap and decreases on the other side of the machine. Therefore, UMP is generated towards the smaller air gap. [7]

The fault is static, which means that the angular position of the minimum air gap stays the same. An asymmetric stator or misaligned rotor can cause the radial eccentricity. These conditions can exist due to manufacturing tolerances or misalignment during assembly. [6]

Radial eccentricity is commonly denoted by relative eccentricity. Relative eccentricity is radial eccentricity proportional to the air gap's length. This means that the same size of radial eccentricity has a different impact on different machines based on their air gap length. Dorrel et al. suggest that 10% of relative eccentricity is approximately the manufacturing tolerance, 30% is a developing fault, 50% is already a very severe fault, and 80% would mean a touchdown level [26]. In this thesis, higher relative eccentricities are used to get more apparent results of different effects of eccentricity.

During radially eccentric operation conditions, the permeance of the machine changes with respect to angle. Figure 3 shows simplified section views of an electrical machine in different operation conditions. [4]

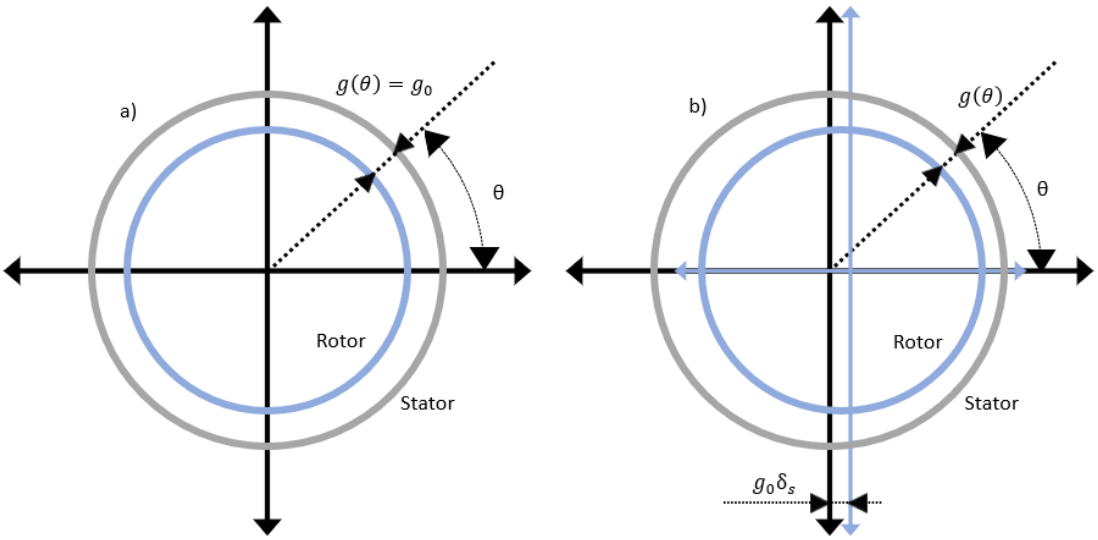

Figure 3: Simplified figure of air gap during (a) normal and axially eccentric situation and (b) static radially eccentric situation. Figure based on [15].

Figure 3 (b) shows how the static radial eccentricity length of δ_s affects the machine's air gap length. Due to static eccentricity, the physical width of the air gap changes around the machine. If the machine is eccentric on the x-axis, the length of an air gap as a function of angle can be depicted by

$$g(\theta) = g_0(1 - \delta_s \cos(\theta)), \tag{27}$$

in which δ_s is the relative eccentricity. Relative permeance caused by eccentricity can be calculated by inserting (27) into (19). Research by Guo et al. derived the permeance generated due to eccentricity (27) further by expanding Fourier's series [27]. Fourier's coefficients can be denoted by

$$\lambda_{e,n} = \begin{cases} \dfrac{1}{\sqrt{1-\delta_s^2}}, n = 0 \\ \dfrac{2}{\sqrt{1-\delta_s^2}} \cdot \left(\dfrac{1-\sqrt{1-\delta_s^2}}{\delta_s} \right)^n, n = 1 \end{cases}, \tag{28}$$

in which $\lambda_{e,n}$ is the Fourier's coefficient. Guo et al. have derived that different permeance harmonics need to be considered depending on the eccentricity's intensity and the num-

ber of pole pairs in the machine. During small eccentricities, the first two coefficients dominate the permeance's magnitude, and with increasing eccentricities, the latter coefficients must be considered. In this thesis, the relative eccentricity used within models is approximately 57.5%. Thus at least the first three components are evaluated. [27] The relative permeance caused by eccentricity will always be over 1, which means that the overall value of the magnetic flux density increases. The increase is also derived by He et al. with an approach based on the power series [7]. They conclude that due to the increasing magnetic flux density, all of the force components in the machine increase due to the static radial eccentricity.

The radial force can be calculated by calculating the radial stress during the eccentric condition and integrating the force based on (24). The resulting force components are

$$F_{\mathrm{x}}(t) = \begin{cases} F_1 \cdot \cos(\theta) + F_4 \cdot \cos(2\omega t - 5\theta), p = 3 \\ f_1 \cdot \cos(\theta), \quad p > 3 \end{cases}, \tag{29}$$

$$F_{\mathrm{y}}(t) = \begin{cases} F_1 \cdot \sin(\theta) + F_4 \cdot \sin(2\omega t - 5\theta), p = 3 \\ F_1 \cdot \sin(\theta), \quad p > 3 \end{cases}, \tag{30}$$

in which F_1 and F_4 are force components. The first represents the constant unbalanced magnetic pull, and the other represents the vibrational component with double the supply frequency. If there are more than 3 pole pairs, the harmonic forces counteract each other. Thus, only the constant UMP remains. [27] Research by Song et al. says that the radial eccentricity may induce harmonic components, which are multiples of pole number to the radial force. These force components are generated only if the machine is rotationally asymmetric. Both machines are rotationally symmetric. Thus, there should not be harmonics caused by the poles on the UMP on either of the machines. [20]

He et al. studied the impacts of eccentricities on electromagnetic torque [15]. Their research concluded that the radial eccentricity would increase the torque's DC component. Research by Song et al. states that the main harmonic components induced by the radial static eccentricity are multiples of pole numbers for the cogging torque [20].

4.2 Axial eccentricity

Axial eccentricity means that the machine's rotor and stator are misaligned axially. As discussed in subchapter 4.2.3, it induces a force which points into the opposing direction of the rotor coming out of the stator body and thus tries to return to the neutral position. The axial eccentricity is determined to be a misalignment of the middle planes of the rotor and stator, and the direction is from the neutral position to the misaligned position. A highly

simplified example is in Figure 4, as well as the axial force opposing the misalignment. Axial eccentricity also affects the other forces even though radially, the machine stays concentric [7].

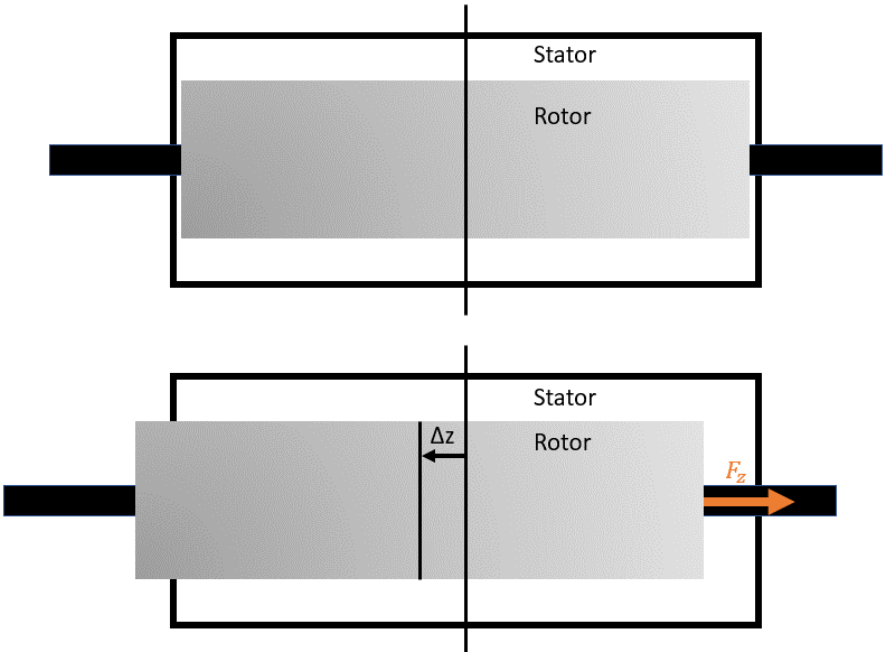

Figure 4: Simplified picture of axial eccentricity.

The axial eccentricity can result from multiple reasons. For example, some traditional generators like steam-, wind- and hydro generators have an axial force due to the prime mover, which may offset the rotor from the stator [7]. Also, if the axis is rigid and the rotor may not centre itself of misalignment due to assembly, there may be an axial eccentricity, which generates force to the bearings. The axial eccentricity affects the forces in two different ways:

- Inducing axial force into the machine
- Reducing the effective length of the machine

The first of the ways is covered extensively in subchapter 3.3.3 as it is the main way that the axial force induces into the machine in the first place. Secondly, by reducing the effective length of the machine, the overall air gap magnetic flux in the machine is reduced. Thus the other force components are reduced [7,22].

The axial eccentricity's effect on the machine's magnetic flux density is studied in He et al.'s research [22]. The study compares magnetic flux densities on the machine's different sides in axially eccentric operation conditions. The magnetic flux density clouds in the study show that the frontend's magnetic flux density stays nearly constant on the stator side, but decreases on the rotor side and vice versa on the backend when the axial eccen-

tricity increases. This means that the magnetic potential difference increases, which means more energy is stored in the air gap. [22] Additionally, the stator current will decrease due to decreasing effective length [22].

If the machine is radially concentric, there should be no net radial force in the machine, but small forces may exist due to the tolerances of the machine. As magnetic flux density decreases due to smaller effective lengths in the machine, these forces also decrease. This means that the radial UMP and vibrations decrease [7]. On the contrary, the axial eccentricity will intensify the axial force and the axial vibrations.

5. METHODS FOR DETERMINING FORCES

There are currently multiple ways of modelling electrical machines researched [1]. The main split between models is if the model is based on analytical models or numerical models such as FEM. Analytical models are based on equations, which calculate the exact values of magnetic and electric variables. FEM is based on splitting the geometry into finite elements. This way, the calculations can be done locally at one point at a time. FEM computes the answers numerically, which means that the solutions will not be exact but approximated to be close enough for practical applications. The main benefits of FEM are the ability to use realistic geometries and to calculate non-linearities [1]. Even the most sophisticated analytical models are still 2D models.

Research focuses on creating analytical models whose results are the same as with FEM. Developing these analytical models is deemed necessary due to the long calculation times in FEM. Still, the models will be evaluated based on FEM results or measurements and FEM results. Analytical models' main benefit over FEM is the reduction of calculation time, but analytical models also create a better understanding of the fundamental factors causing the results given by FEM. [8] Due to the complexity and time required to create an accurate enough analytical model, it is not being done in the scope of this thesis. Instead, FEM results of simplified models are used to calculate approximations, which would be close to the results of more complex FEM simulations.

This chapter includes specifications of the machines used in this thesis, 2D and 3D models. FEM models are used in this thesis to calculate electromagnetic fields and forces within the machine. Two selected machines are modelled in 2D and 3D with Altair Flux software. This software is selected as it is already being used at Yaskawa Lappeenranta for electromagnetic calculations.

5.1 Machine data

In this chapter, both PMSM machines' specifications are briefly examined and compared. FEM geometry must fulfil these specifications. Table 1 contains geometrical data, which is used to build up the models.

Table 1: Machine data for the two different machine types.

	PMM500	PMM1500	Unit
Stack active length	800	840	mm
Rotor diameter	570	1893	mm
Number of partial stacks	16	12	
Physical air gap	3.5	6	mm
Number of stator slots	54	192	
Number of pole pairs	3	16	
Rotation speed	1440	65	rpm
PM location	Embedded	Surface	

PMM500 represents the internal permanent magnet machine, and PMM1500 is the surface permanent magnet machine. Machines' sizes differ significantly as the diameter of the PMM500 is approximately 2 times larger than the PMM500's diameter. Also, the rotation speeds vary significantly as PMM500's rotation speed is about 21 times larger than the PMM1500 machine. Such speeds cannot be done on surface mounted rotors as the magnets would experience too high centrifugal forces, leading to them detaching from the rotor body.

5.2 2D-FEM geometry

2D modelling of electrical machines is the standard method currently used in the industry. The main benefit of FEM is accurate geometry, which can be altered to calculate changes in operation. This removes the requirement to build multiple prototypes, and the built machines' operational data is already known. The only real simplification in the radial 2D model is that the geometry is infinitely deep perpendicularly to the machine face. The calculations are done within a certain length of this depth. This means that the end parts of the machine are not accounted for in calculations. Traditionally, also the geometry is simplified to account for only one pole as in electrical machines, every pole is symmetrical in normal operation. An example of a single-pole 2D model is in Figure 5.

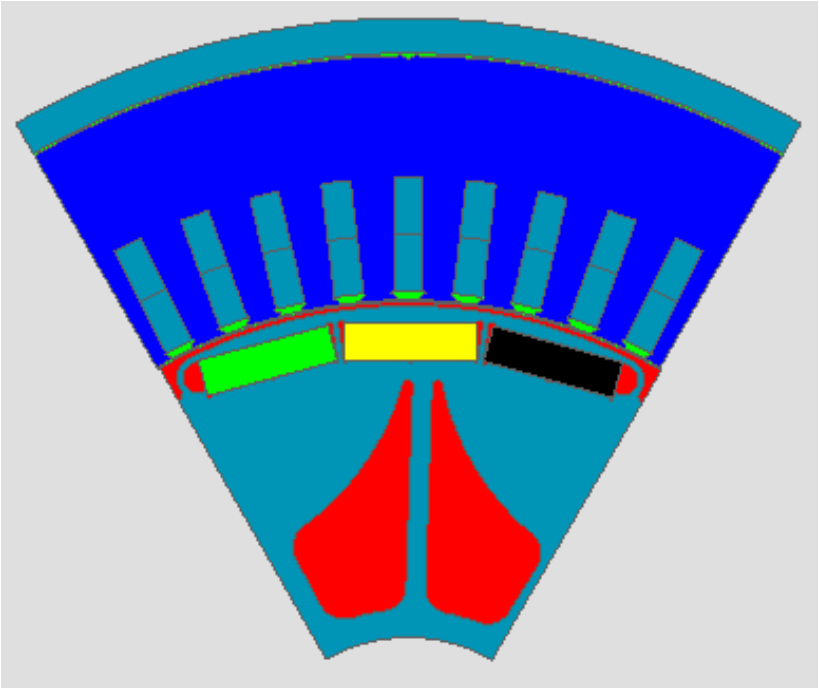

Figure 5: Geometry of a rotor pole of PMM500 machine.

The basic model includes rotor and stator geometry, and it can be used to calculate all electromagnetic data required in basic operation. During static radially eccentric operation, the air gap width is a function of the angular coordinate within the machine. For this reason, a single-pole model cannot be used anymore, but the whole machine face must be modelled. An example of a full machine model is in Figure 6.

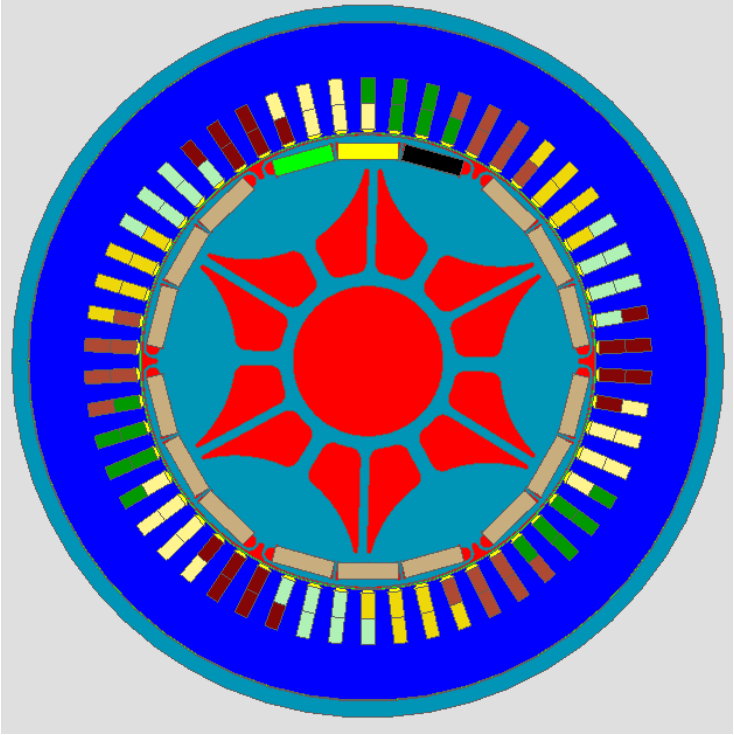

Figure 6: Full machine 2D model of the PMM500 machine.

The radial symmetry can be seen in Figure 6. Building the whole model significantly increases the computational time compared to a single-pole model due to the increase in size. The model has been made so that the rotor can be moved in any direction in a 2D plane. As previously stated, the 2D model is thought to be a part of an infinitely long machine. Even though axial eccentricity decreases the operational axial length of the machine, just changing the depth of the 2D model is not sufficient. This is due to axial eccentricity changing machines' operating positions differently from different sides of the machine. On one end, the stator is further than the rotor, and on the other end, vice versa, which results in axial forces. The 2D model would approximate the rotor and the stator to be the same length, which would mean that the effects of axial force could not be seen from the calculated data. Furthermore, the axial force could not be calculated at all.

5.3 3D-FEM geometry

3D models can be expanded from 2D models, which means that exact calculations with full geometries can be done. This comes with a drawback, as larger models equal more elements. Thus, calculations take longer. The main benefit of 3D models comes with the addition of a third dimension. This allows the software to use exact equations and not the equations simplified to 2D. Other benefits include the addition of skewing, the ability to calculate magnetic reactions on the ends of the machine and an even better geometrical representation of the modelled machine. In Figure 7 are pictures of PMM500's 2-stack and 4-stack models, and in Figure 9 is a picture of the PMM1500's model.

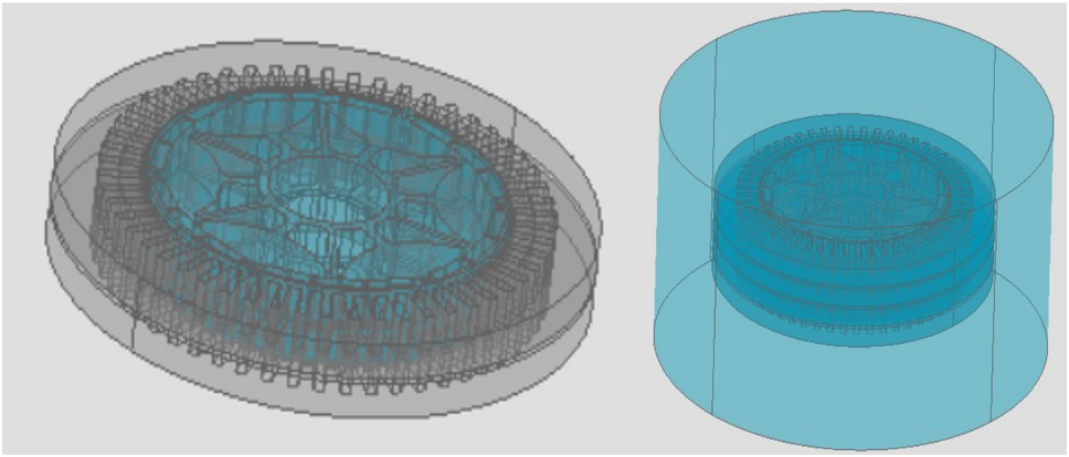

Figure 7: 2-stack and 4-stack models of PMM500 machine.

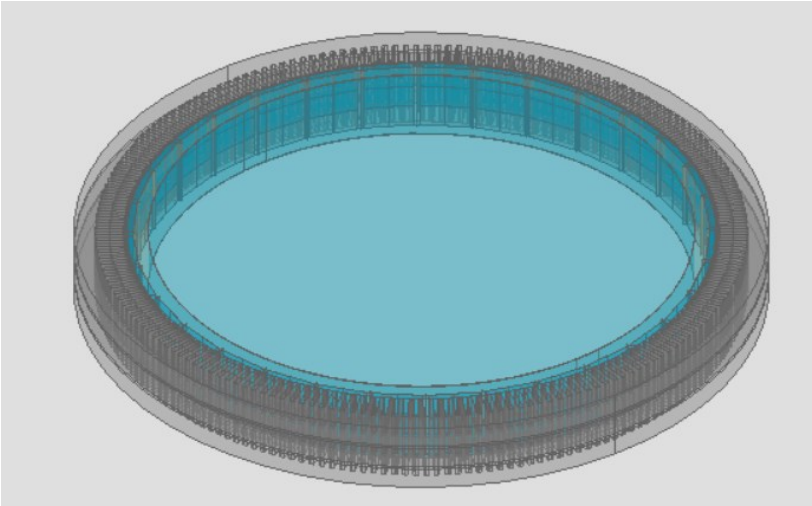

Figure 8: Single magnet module model of the PMM1500 machine.

The figures show that both models are shortened to include only some stacks. These simplifications had to be done as longer models could not have been modelled due to restrictions of the used computer's specifications. PMM500 has been 3D-modelled with 2 stacks and 4 stacks as the same skewing would represent the full machine's skewing by including the same amount of skewed and non-skewed stacks. Table 2 contains the data of all created models. No other simplifications had to be done to represent the PMM500 model. The 3D model of PMM1500 includes only one magnet module, and the band holding the magnets had to be removed. The skewing in the PMM1500 machine is realised by rotating the magnet modules. Thus, the skewing could not be considered in the model.

Table 2: Created FEM-models during this thesis.

Machine type	2D	3D
PMM500	Full machine	2 and 4 stacks
PMM1500	Full machine	1 magnet module which contains 3 magnets

5.4 Axial force measurements

Axial forces have been measured for the PMM500 machine previously by Yaskawa. The measurements were done in their facilities, and the principle of the test was to move the rotor to a certain displacement and then measure the force required to create the displacement. Table 3 contains results for the measured force with respect to eccentricity for a warm machine.

Table 3: Measurement data of PMM500 machine.

Eccentricity: [mm]	Measured force: [N]
0	6
0.51	484
1.01	940
1.51	1365
2	1745
2.5	2090

The force created by the eccentricity is quite linear, and the tests did not reach the saturation point mentioned by the studies [14,21].

5.5 Analytical axial force calculations

The analytical method created during this thesis is based on simplifying the flux flows and using normal stress to approximate axial forces. The calculation method was created based on wishes from Yaskawa. It needed to be a simple method based on physical parameters which can be changed to represent other machine models. Calculation parameters are listed in Table 4.

Table 4: Calculation parameters for analytical axial force model.

Parameter	Unit
Rotor diameter, D_{ri}	mm
Width of stator slot, w_{ss}	mm
Width of permanent magnet, w_{PM}	mm
Width of cooling duct, w_{cd}	mm

Height of physical air gap, g_0	mm
Number of pole pairs, p	
Number of stator stacks, ss	
Normal stress, $\sigma_{\mathbf{pole,rad}}$	Pa

Physical dimensions are based on the machine parameters, and normal stress across the magnet is calculated based on magnetic flux density given by radial 2D FEM calculations. The calculations are done based on Figure 9, which shows most of the required dimensions for the calculations.

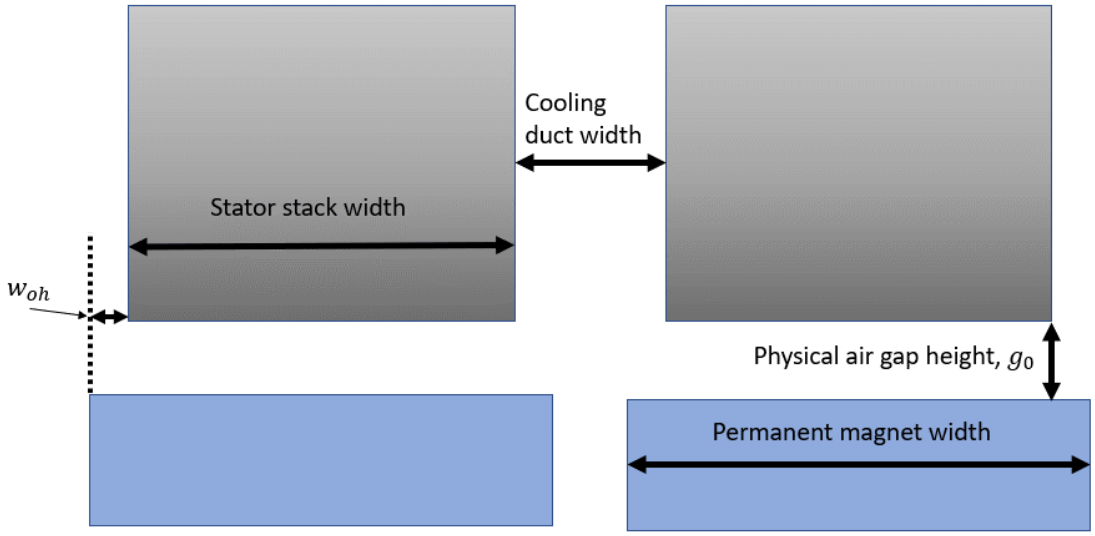

Figure 9: Physical dimensions for an analytical axial force calculation.

Figure 9 shows two partial stacks of a machine, including two separate stator stacks and two permanent magnets. The main dimensions can be measured from the machine based on Figure 9. Both calculated machines have magnets wider than the stator stack, and the equations are based on resembling that. Calculations are simplified by not taking harmonics and tangential forces into account, and the calculations can be divided into 6 parts:

1. Calculate normal stress over a pole with FEM software in a magnetically neutral position.

2. Calculate the sum of the absolute values of normal stress over one pole

Normal stress over one rotor stack can be calculated with

$$\sigma_{\mathrm{rs,rad}} = 2p\sigma_{\mathrm{pole,rad}}, \tag{31}$$

in which $\sigma_{\mathrm{rs,rad}}$ is the normal stress over rotor stack and $\sigma_{\mathrm{pole,rad}}$ is the normal stress over one pole.

3. Displace the magnet with Δz and calculate how much the average air gap length changes due to displacement.

Calculate how much the magnet edges go past the stator stack's edges.

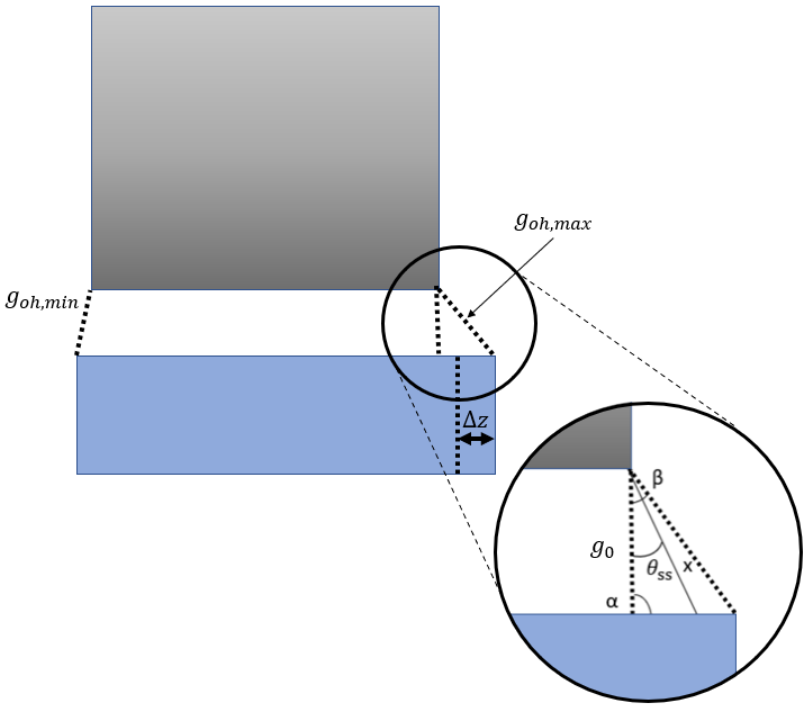

Figure 10: Physical meanings for magnet displacement.

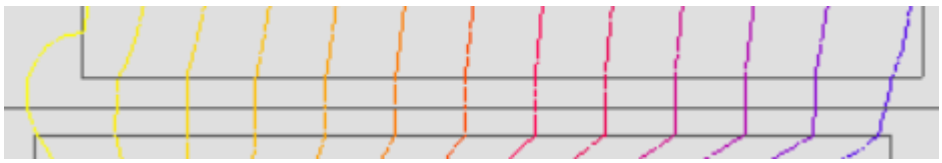

Figure 11: Flux lines between magnet and stator teeth on embedded magnet machine.

Based on Figure 11, it was concluded that the magnetic flux flows nearly linearly across the air gap if the magnet is under the stator slot. Distance from the stator slot's edge to a point over the edge of the permanent magnet can be calculated with

$$x(\theta_{\mathrm{ss}}) = \mathrm{g}_0 \frac{\sin(\alpha)}{\sin(\alpha + \theta_{\mathrm{ss}})}, \tag{32}$$

in which x is the length to a point on the permanent magnet, θ_{ss} is the angle between x and g_0, and α is the angle between the closest point of a permanent magnet and a line from the stator slot's edge to the closest point of a permanent magnet. If the permanent magnet is under the stator slot α value is $\frac{\pi}{2}$. By integrating the angle θ_{ss} from the closest point of the magnet to $g_{\mathrm{oh,min/max}}$ and dividing with the maximum angle, we can calculate the average value of x.

$$x_{\mathrm{avg}} = \frac{1}{\beta} \cdot \int_0^{\beta} a \cdot \frac{\sin(\beta)}{\sin(\beta + \theta_{\mathrm{ss}})}, \tag{33}$$

in which x_{avg} is the average value of *x*'s length and β is the maximum angle used on the integration. The average air gap length of a single permanent magnet under a stator slot can be calculated with

$$\mathrm{g}_{\mathrm{avg}} = \begin{cases} \frac{w_{\mathrm{oh}} - \Delta z}{W_{\mathrm{PM}}} \cdot \left(x_{\mathrm{avg,min}}\right) + \frac{w_{ss}}{w_{\mathrm{PM}}} \cdot g_0 + \frac{w_{\mathrm{oh}} + \Delta z}{W_{\mathrm{PM}}} \cdot \left(x_{\mathrm{avg,max}}\right), \ \Delta z \ \leq w_{\mathrm{oh}} \\ \frac{w_{ss} + (w_{\mathrm{oh}} - \Delta z)}{w_{\mathrm{PM}}} \cdot g_0 + \frac{w_{\mathrm{oh}} + \Delta z}{W_{\mathrm{PM}}} \cdot \left(x_{\mathrm{avg,max}}\right), \Delta z \ > \ w_{\mathrm{oh}} \end{cases}, \tag{34}$$

in which $\mathrm{g}_{\mathrm{avg}}$ is average air gap length, $x_{\mathrm{avg,min/max}}$ are average air gap lengths of the parts of magnet, which are not under the stator slot, w_{oh} is the part of permanent magnet that overhangs the rotor during magnetically neutral position, w_{ss} is the width of the stator slot and Δz is the displacement. The average air gap length is weighted based on the proportions of the magnet.

4. Calculate new normal stress based on the increased length.

Increasing air gap length decreases permeance, altering the air gap's magnetic flux density. Based on (9) and (19), it can be approximated that the normal stress due to increased relative permeance can be calculated with

$$\sigma_{\mathrm{rs,rad},\Delta z} = \left(\frac{g_0}{g_{\mathrm{avg}}}\right)^2 \cdot \sigma_{\mathrm{rs,rad}}, \tag{35}$$

in which $\sigma_{\mathrm{rs,rad},\Delta z}$ is the new normal stress due to changed permeance.

5. Calculate the area of the magnet that is displaced and multiply it by the number of stator stacks.

Previous steps have been calculated for a single permanent magnet and a stator stack. Displacement happens in all the stacks, and as the stacks are symmetrical, the overall area is multiplied by the number of stacks. The displaced area can be calculated with

$$\mathrm{A}_{\Delta z} = \pi D_{\mathrm{ri}} \cdot \Delta z \cdot ss\,, \tag{36}$$

in which D_{ri} is the diameter of the rotor and ss is the number of stator slots.

6. Calculate the force, which is caused by the area of displacement.

Magnetic force can be calculated based on Maxwell's stress theory, as discussed in chapter 3.3.1. Axial force can be calculated based on (22) by approximating that the area of displacement is the cause of an axial force. The equation of axial force is

$$\mathrm{F_z} = \sigma_{\mathrm{rs,rad,\Delta z}} \cdot \mathrm{A}_{\Delta \mathrm{z}}, \tag{37}$$

in which $\mathrm{F_z}$ is axial force.

For comparison, the axial force calculation method by Bradford and Rhudy is presented [21]. In their method, the force is split into four components. Two components consider the displacement of alignments between stator's and rotor's endings and ventilation ducts. The third component considers the skew of the machine, and the last component considers the interaction between the end turns of the rotor winding, which can be neglected in PMSM as there are no rotor windings. These components can be used to calculate axial force with

$$F_z = 1.32245 \times a_{\mathrm{ph}} \left(\frac{60}{f}\right) \frac{E_0 I_{\mathrm{m0}}}{L_0} \left(\frac{L_0}{L}\right)^2 \times \left(\frac{\partial L}{\partial z}\right), \tag{38}$$

in which a_{ph} is the number of phases, f is the main supply frequency, E_0 is the phase voltage, I_{m0} is the phase current, L is the effective length of the rotor, which means the length of the rotor (L_0) minus displacement, and $\left(\frac{\partial L}{\partial z}\right)$ is the rate of change between the displacement and rotors effective length. [21] Equation (38) is modified from the equation presented by Bradford and Rhudy by changing the units to SI-units [22]. Additionally, $\left(\frac{\partial L}{\partial z}\right)$ can be written as $\left[\frac{2}{\pi} ctn^{-1}\left(\frac{\Delta z}{g_o}\right) - 1\right]$ by doing a Schwarz-Christoffel transformation to the idealized stator and rotor end surfaces [21].

6. RESULTS

Both 2D and 3D models of both machines have been created. 2D models are used to calculate radial forces, and 3D models for axial forces. Both models are computed in no-load conditions. The resultant forces are further analysed with FFT to calculate the forces' fundamental component and harmonic content so that they can be compared to concentric operation conditions. 3D models do not include the whole machine due to technical restrictions with Altair Flux software.

6.1 Results from radial eccentricity

Radially eccentric operation conditions affect magnetic flux density, radial force, and torque, as discussed in chapter 4.1. 2D-FEM is used to calculate operating conditions and forces during the radial eccentricity. Results of a no-load condition are modelled, and eccentricity is modelled by offsetting the rotor. Both machines are modelled with approximately 57.5 % relative eccentricity.

Eccentricity's main result should be increasing the radial forces DC-component, increasing the overall magnetic flux density, increasing torque harmonics, and inducing new harmonics to forces.

6.1.1 The effect of radial eccentricity on the magnetic flux density

Eccentricity's effect on magnetic flux density is covered mathematically in subchapter 3.2, and this chapter focuses on analysing the results of the FEM software. Figure 12 contains magnetic flux density distributions of the PMM500 machine during normal and eccentric operating conditions.

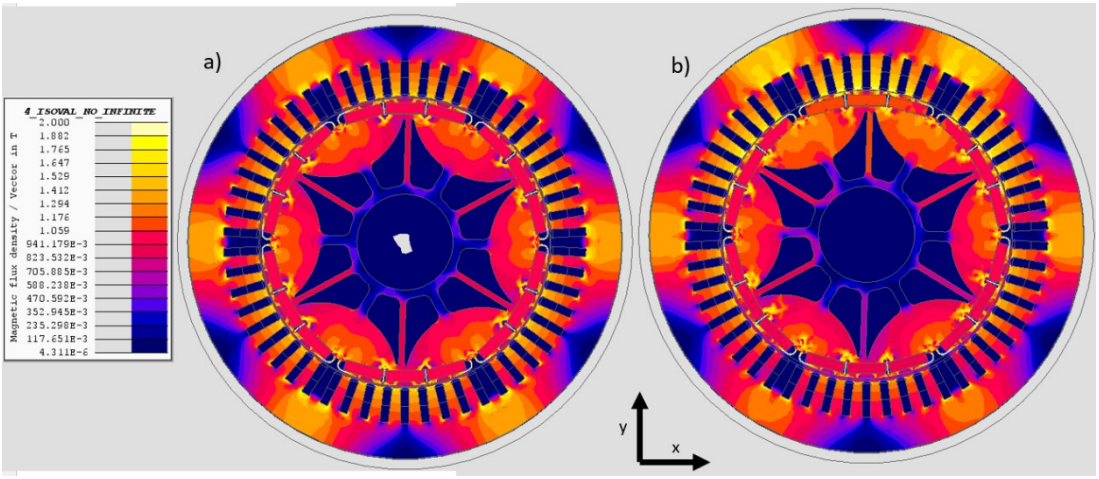

Figure 12: Magnetic flux density of the PMM500 machine during (a) concentric operation condition and (b) eccentric operation condition.

The grey part in Figure 13 (a) is an area with a lower flux density than the lowest value on the scale, and the rotor is offset from the stator towards the positive y-axis. Figure 12 shows the periodicity of the machine as the flux densities across a pole are identical. The flux density increases on the minimum air gap side, which can be seen as brighter colours on the upper part of the Figure 13 (b) and decreases on the lower part. This change does not apply only to the air gap, but overall, the flux density levels change even though the flows do not change drastically from the concentric operation condition. Figure 13 and Figure 14 depict the air gap flux densities of PMM500 and PMM1500, respectively. Table 5 covers the overall average air gap flux densities and their changes with induced eccentricity.

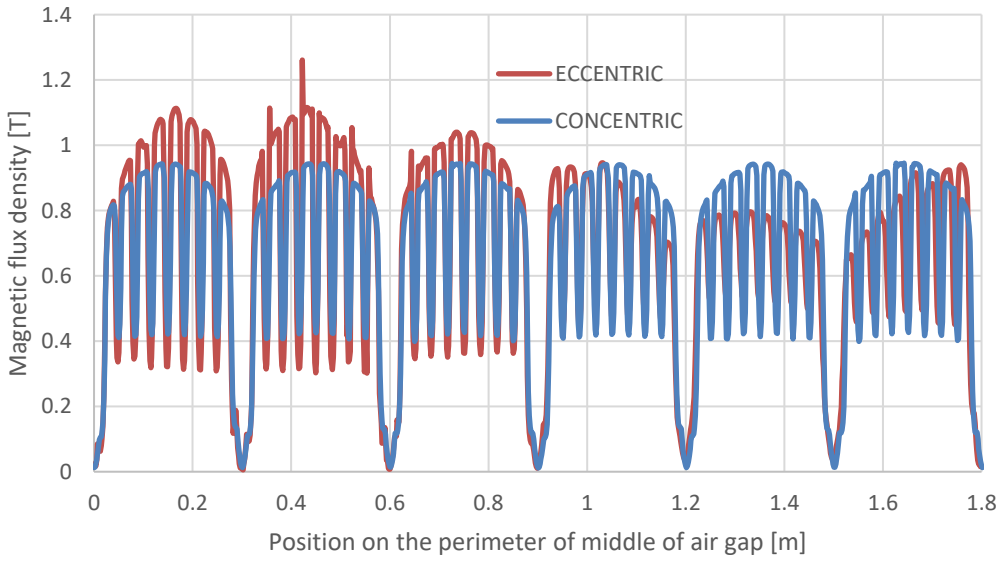

Figure 13: Absolute value of airgap's magnetic flux density during concentric and eccentric conditions on the PMM500 machine.

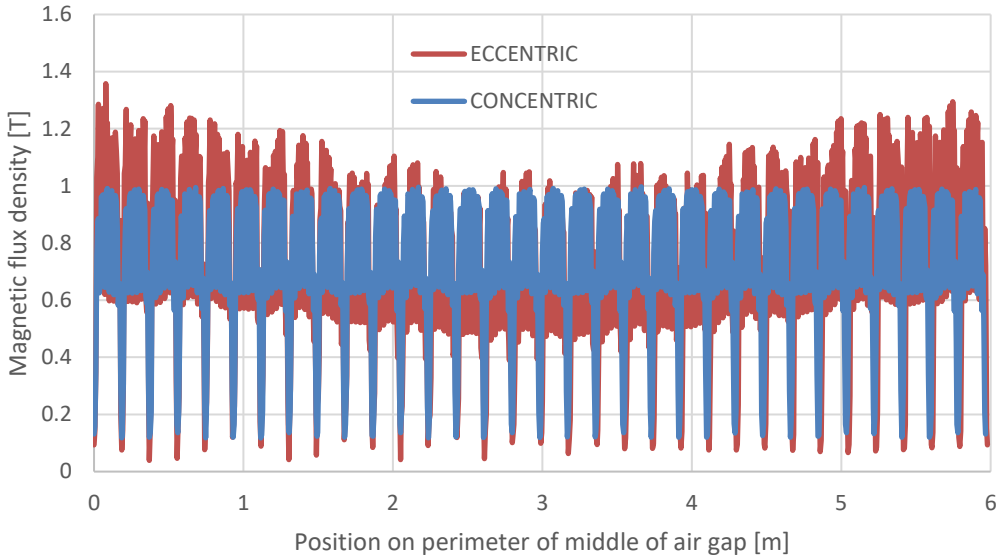

Figure 14: Absolute value of airgap's magnetic flux density during concentric and eccentric conditions on the PMM1500 machine.

The permanent magnets create the magnetic flux densities, as seen on both figures. The magnetic flux density is higher on the side of the smaller air gap due to the eccentricity. The overall intensity of the flux density can be approximated by taking the average rectified value (ARV) of the magnetic flux density.

Table 5: Comparison of magnetic flux densities in concentric and eccentric conditions.

	ARV Concentric: [T]	ARV Eccentric: [T]	Increase:
PMM 500	0.658977	0.663283	0.65 %
PMM 1500	0.731785	0.743198	1.54 %

Table 5 shows that both machines' flux densities increase by a little. This should result in larger forces across the machine.

6.1.2 The effect of radial eccentricity on the radial force

The radial force of PMM 500 is in Figure 15, and PMM 1500 is in Figure 16. Both figures depict a normal operating condition and an eccentric operation condition with respect to a rotating rotor. The rotor is rotated over one electrical cycle of the machine, and the rotation's angular position denotes the rotation. Eccentricity depends on the machine type, as the air gap width differs between machines. The relative eccentricity is selected to be approximately 57.5 % for both machines.

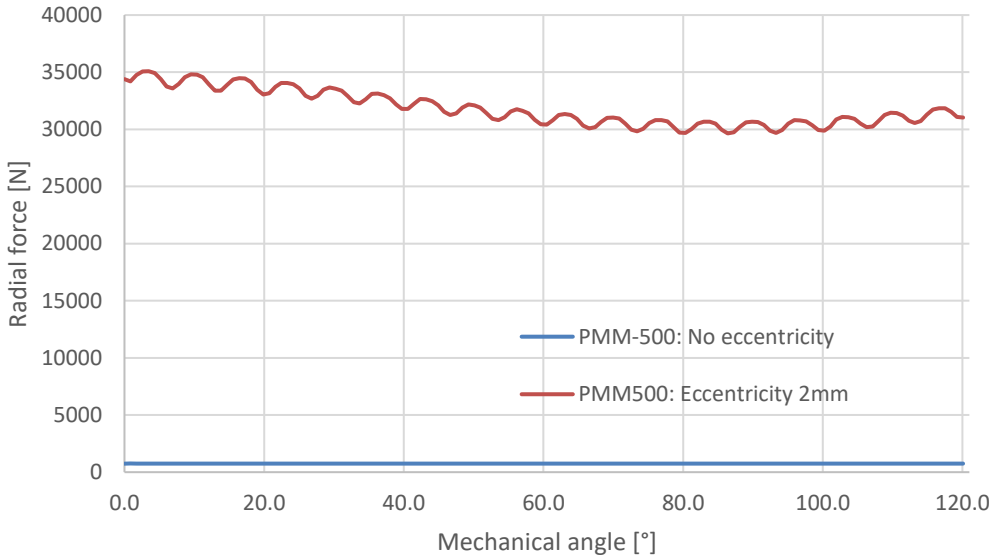

Figure 15: Radial force of PMM500 machine during concentric and eccentric conditions.

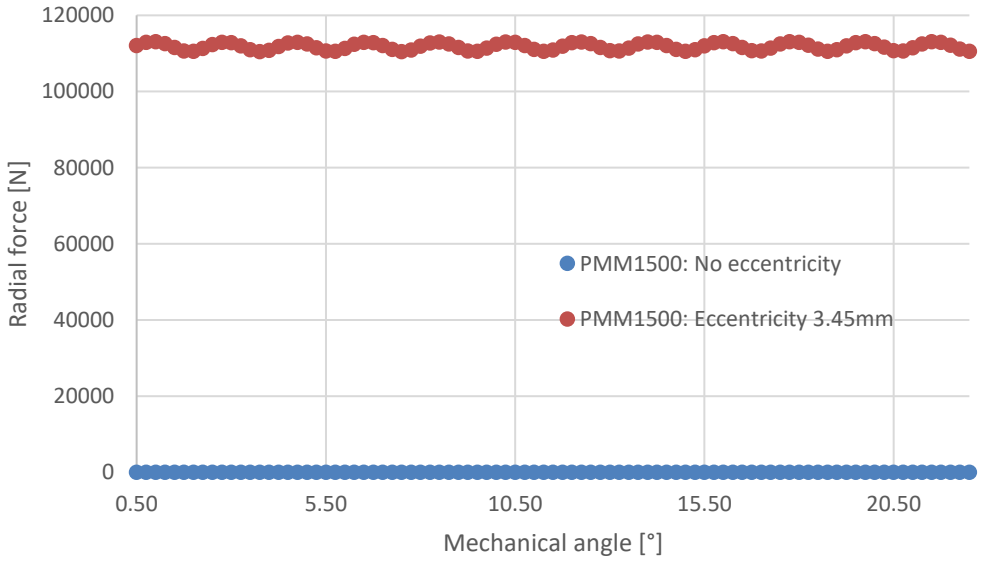

Figure 16: Radial force of PMM1500 machine during concentric and eccentric conditions.

There is a small radial force during the normal operating condition in the PMM500 machine. This may be due to uneven meshing of the machine or geometric defects in the model. The force rotates according to the machine rotation, implying either uneven magnetisation or dynamic eccentricity within the created model. Force's amplitude and the direction of the force during concentric condition can be seen in Figure 17.

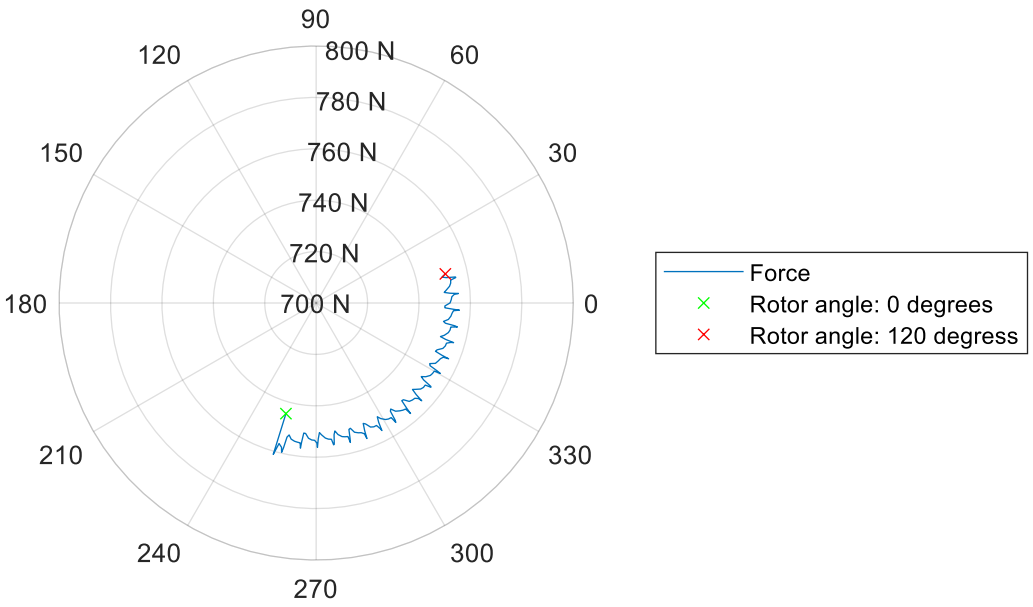

Figure 17: Circular representation of PMM500's force during the concentric condition.

Figure 15 and Figure 16 show drastic increases in radial force when eccentricity is added to the models. The main increase is in the DC component. The radial forces DC components of both machines are listed in Table 6.

Table 6: Radial forces with different eccentricities for both machine types.

Eccentricity: [mm]	Relative eccentricity: [%]	PMM500: [kN]	Relative eccentricity: [%]	PMM1500: [kN]
0	0	0.75	0	0.00
0.5	14	7.83	8	16.07
1	29	15.45	17	32.10
1.5	43	22.96	25	48.22
2	57	30.62	33	64.29
2.5	71	38.71	42	80.40
3	86	47.53	50	96.50
3.5		-	58	112.6
4		-	67	129.7

Table 6 shows that the radial force increases nearly linearly, with increasing radial eccentricity. PMM500 machine's radial force increases 7 to 8 kN, and PMM1500 machine's approximately 16 kN for a 0.5 mm increase in eccentricity. Additionally, sinusoidally varying excitations are induced to the radial force on both machines. Sinusoidal components are further analysed with a fast Fourier transform (FFT). FFT of PMM500's radial force can be seen in Figure 18 and FFT of PMM1500's radial force can be seen in Figure 19, without DC components. DC components are not included as their amplitude would decrease the visibility of amplitudes of higher order harmonics. The radial eccentricity calculations follow the study conducted by Song et al., where harmonic components of UMPs and cogging torques are calculated over an entire mechanical cycle [20]. One complete mechanical cycle is modelled for the PMM500 machine with steps of 1 degree. For the PMM1500 machine, only a quarter of the mechanical cycle is modelled with steps of 0.25 degrees.

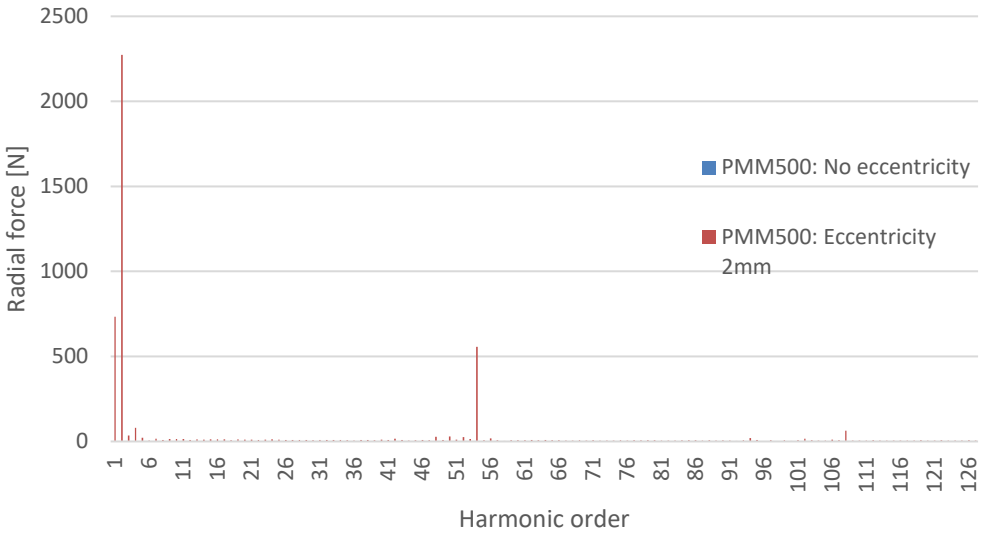

Figure 18: Radial force spectrum of PMM500 machine during concentric and eccentric conditions.

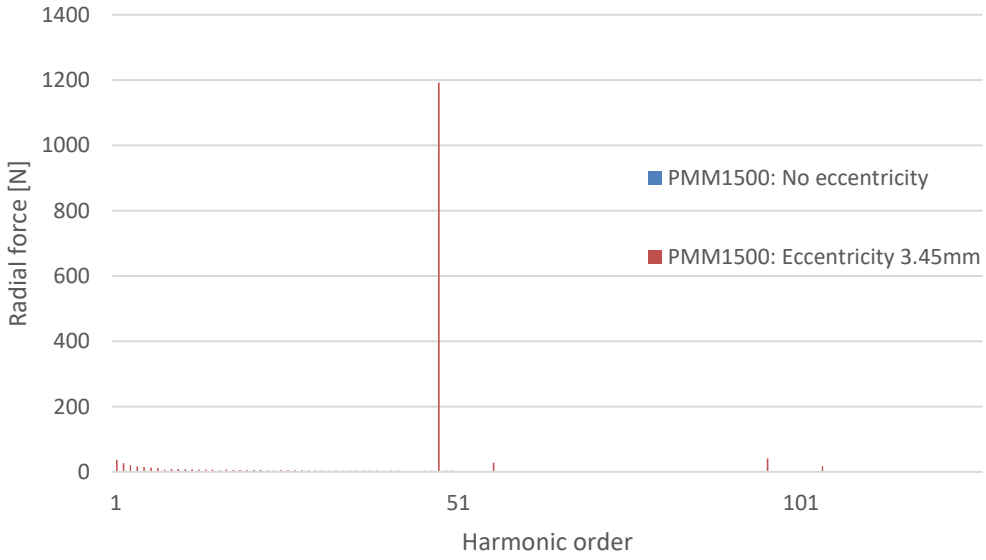

Figure 19: Radial force spectrum of PMM1500 machine during concentric and eccentric conditions.

Both figures include radial force harmonics during normal operation situations, but they can barely be seen because they are so small. This means that all the harmonics are induced by eccentricity. Figure 18 shows harmonic force components on the 1st, 2nd, 4th, and 54th harmonic orders. 1st and 4th harmonic components are created by the uneven magnetisation or dynamic eccentricity [20]. The amplitude of the 1st component is the same as the offset during the non-eccentric condition. The 2nd harmonic component is induced by the eccentricity, which was derived in chapter 4.1. The stator slots induce 54th component, but due to the rotational symmetry of the rotor pole, harmonics are not induced in either of

the machines. Only a quarter of the force wave is modelled for the PMM1500 machine, the harmonic orders are one-quarter of the actual harmonic components. Thus, the 48th harmonic component represents the component induced by the lowest common multiple of the number of poles and the number of stator slots. None of the other components is as impactful. Notably, a difference in the lower harmonic components can be seen as no 1st, and 2nd harmonics are induced. In chapter 4.1 was concluded that if there are more than 3 pole pairs, the created harmonic forces with 2 times the supply frequency do not exist. Additionally, the 1st order component is not generated as the model's geometry has no faults.

6.1.3 The effect of radial eccentricity on the torque

The torque of the PMM500 can be seen in Figure 20 and of the PMM1500 in Figure 21. Both torques are calculated using the same eccentricities as on radial forces.

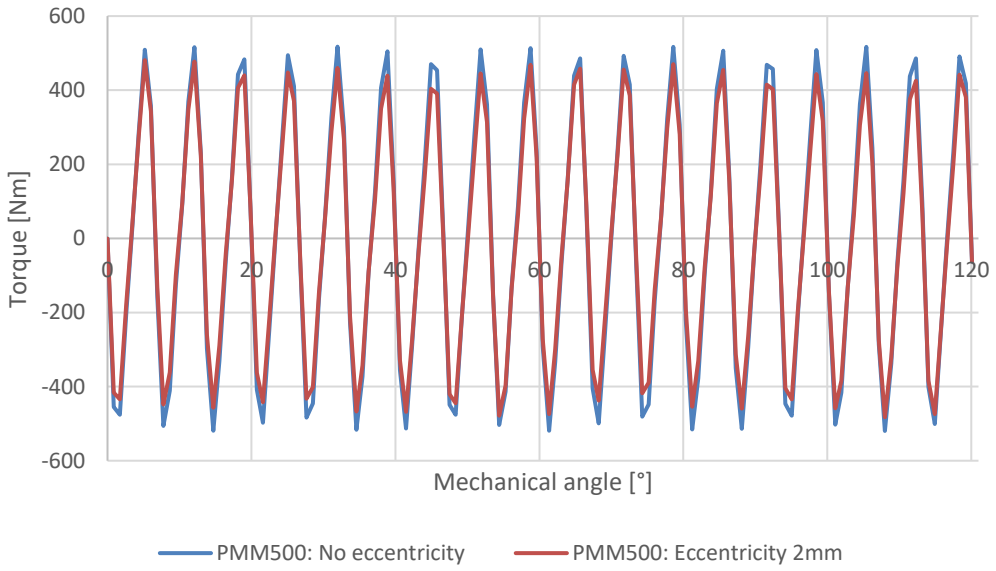

Figure 20: FEM results of PMM500 machine's torque during concentric and eccentric conditions.

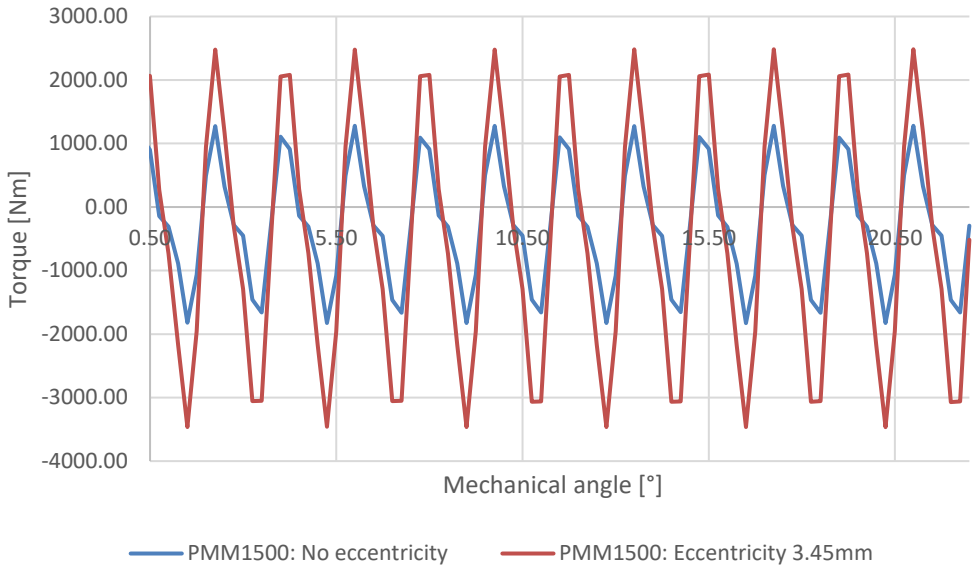

Figure 21: FEM results of PMM1500 machine's torque during concentric and eccentric conditions.

The figures show that the torque vibrates mainly with the same frequency with or without eccentricity, but amplitude varies. Both machines are modelled on no-load conditions. The torque's DC components are 0, and the torque seen is only based on the cogging torque. On the PMM500, machine cogging torque decreases with increasing eccentricity, and on the PMM1500 machine, it increases. By applying the FFT to torque, curves can be split into harmonic components. The FFT of the PMM500s cogging torque can be seen in Figure 22, and the FFT of the PMM1500s torque can be seen in Figure 23.

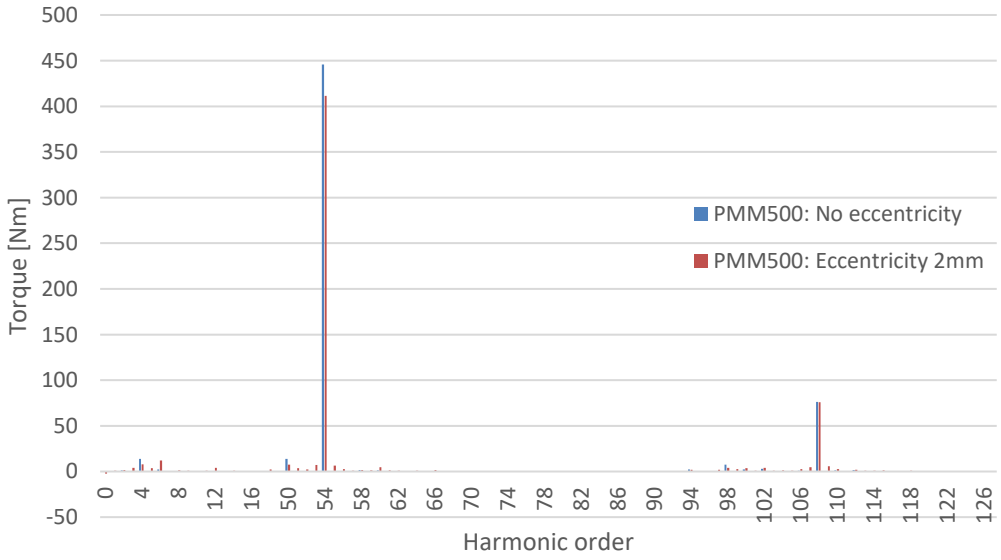

Figure 22: Torque spectrum of PMM500 machine during concentric and eccentric conditions.

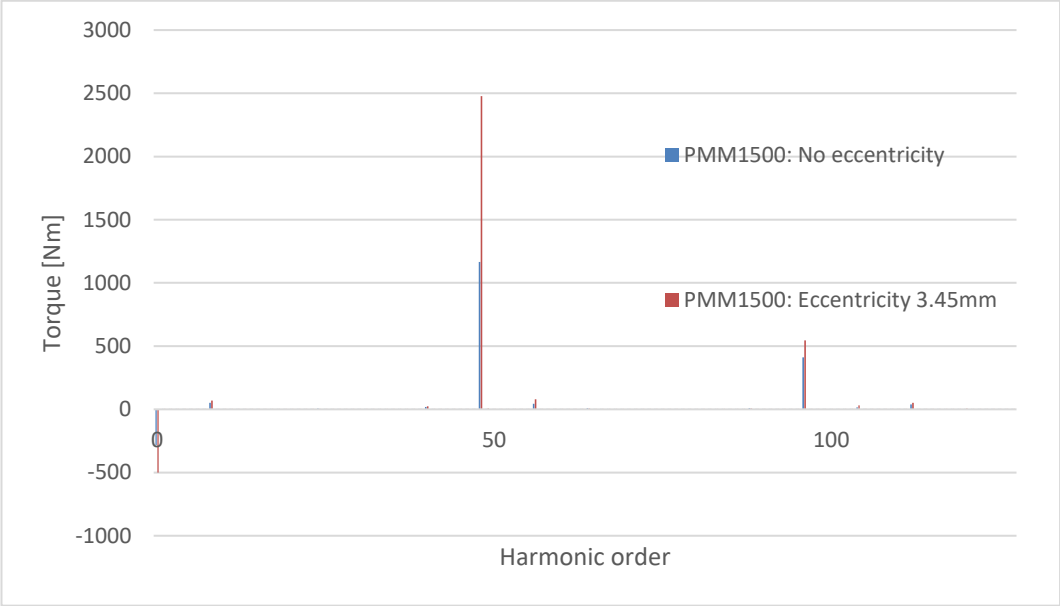

Figure 23: Torque spectrum of PMM1500 machine during concentric and eccentric conditions.

The torque's main vibration orders are 54th harmonic on the PMM500 and 48th on the PMM1500 during both operating conditions. The torque vibrates due to lowest common multiple of stator slots and poles in the concentric condition and due to lowest common multiple of stator slots and poles and rotor poles during the eccentric condition. The eccentricity induces pole harmonics, which can be seen as a 6th harmonic order on the PMM500's distribution and an 8th harmonic order on the PMM1500 distribution. The amplitudes of the fundamental harmonics differ between the machines. The amplitude of the PMM1500 follows the principles discussed in chapter 3.3.2 but PMM500s cogging torque amplitudes decrease with increasing eccentricity.

6.2 Results from axial eccentricity

Axial eccentricity affects magnetic flux density, torque, and radial and axial forces, as discussed in subchapter 4.2. The axial eccentricity's effects are simulated with 3D models. Results from the model of the PMM1500 machine could not be fully calculated with the created model due to time constraints. Thus, most of the results covered in this chapter cover the results from the PMM500 machine. The results of the 3D models and the measurements are used as a baseline to verify an analytical tool that calculates approximations of the axial forces. The analytical tool is compared to the FEM results and the measurements. No-load condition is modelled both for the concentric and the axially eccentric machine.

The literature review concludes that the axial eccentricity increases the axial forces but decreases radial forces and torque. Additionally, axial force should induce axial vibrations into the system.

6.2.1 The effect of axial eccentricity on the magnetic flux density

In Figure 25 are magnetic flux density distributions of both ends of the PMM500 machine in axially eccentric conditions. For comparison in, Figure 24 is the magnetic flux density during the non-eccentric condition.

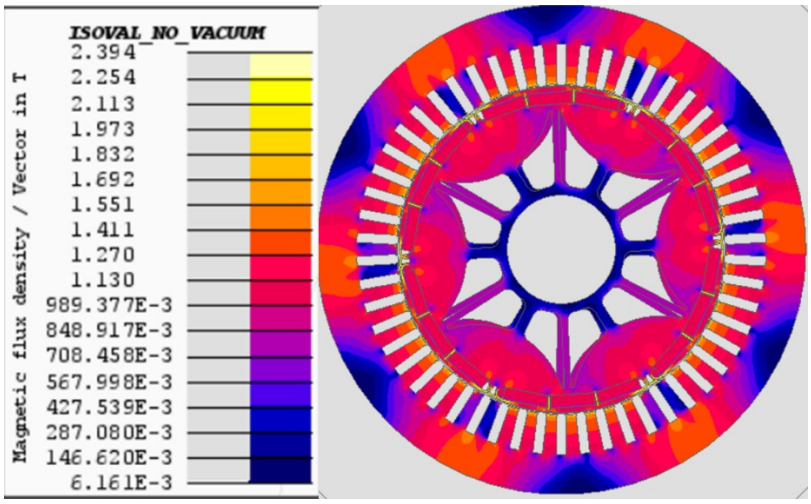

Figure 24: The magnetic flux density distribution of the PMM500 machine during the non-eccentric condition.

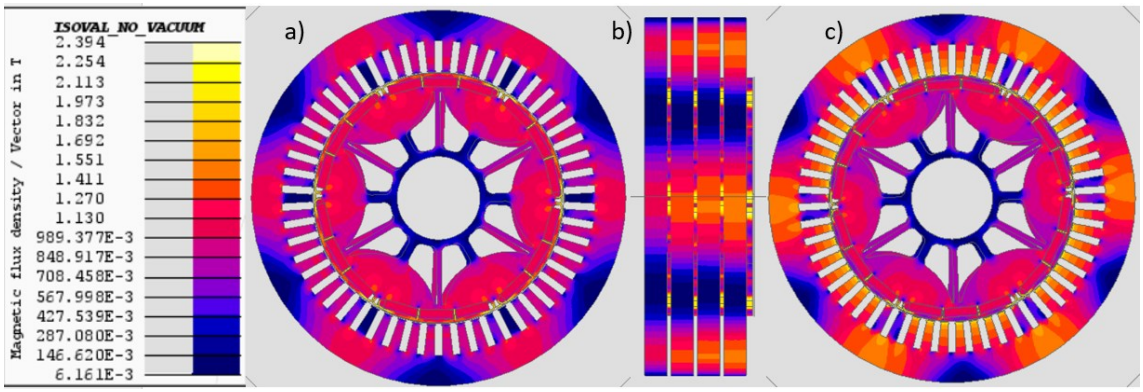

Figure 25: The magnetic flux density distribution of the PMM500 machine during 15mm axial eccentricity condition, in which (a) depicts the plane, where the rotor moves into the stator body, (b) depicts a side view and (c) depicts the plane, where the rotor moves out of the stator body.

The figures show changes in the magnetic flux density. The effect of axial eccentricity on magnetic flux density depends on which end of the machine is analysed. On the side where

the rotor's end is moving closer to the middle plane of the machine, the stator's magnetic flux density decreases significantly, whilst the rotor's magnetic flux density stays the same or increases slightly compared to the non-eccentric operation condition. The stator's magnetic flux density increases continuously in the middle, moving towards the side, where the rotor pushes out of the stator body. On this side of the machine, the magnetic flux density of the stator seems to peak, with a slight increase compared to non-eccentric operation condition. The rotor's magnetic flux density has decreased. These results follow the results obtained by He et al. in their research [22]. Additionally, the magnetic flux density changes gradually from another end of the machine to the other end.

6.2.2 The effect of axial eccentricity on the radial force

The created 3D models are radially concentric, so any radial force should not affect the machine. Even then, there is a small radial force affecting the PMM-500 machine during concentric operation condition, which can already be seen in the results of the 2D model. Therefore, the effect of axial eccentricity on this force can be evaluated. PMM500's radial force with respect to axial eccentricity can be seen in Figure 26. Figure 26's values were calculated with 3D FEM, and the model used for the calculations was a 4 stack model.

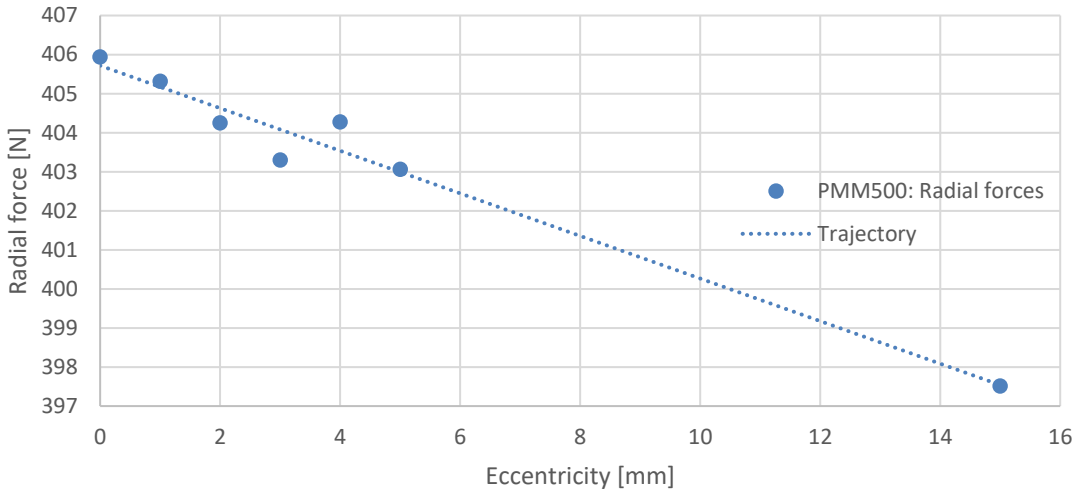

Figure 26: PMM500's radial force with respect to axial eccentricity.

Figure 26 shows radial forces values, with different axial eccentricities and the downwards trajectory of the radial force. As can be seen, the radial force is very small as there is no eccentricity induced radially. Due to the force being small, eccentricity affects the force only by a few newtons. Even though the calculated values are based on the single position of the rotor, the force may fluctuate up to 2 N due to harmonics or unoptimized mesh. For that reason, a single position with 15 mm eccentricity was calculated as well. The value fits

well with a linear regression of calculated values and shows that the force decreases with respect to eccentricity. The difference in forces is very small. The computed results follow the results obtained by He et al. [7]. In their study, changing the axial eccentricity from 4 mm to 6mm during mixed eccentricity changed the radial force's DC-component by 1.28 %, within this study, the change is 0.4 % for 2 mm eccentricity for the PMM500 machine.

6.2.3 The effect of axial eccentricity on the torque

Similarly to the radial force, the cogging torque should slightly decrease due to decreasing axial length. Torque values of the PMM500 machine during axially centred and with 1 mm eccentricity can be seen in Figure 27.

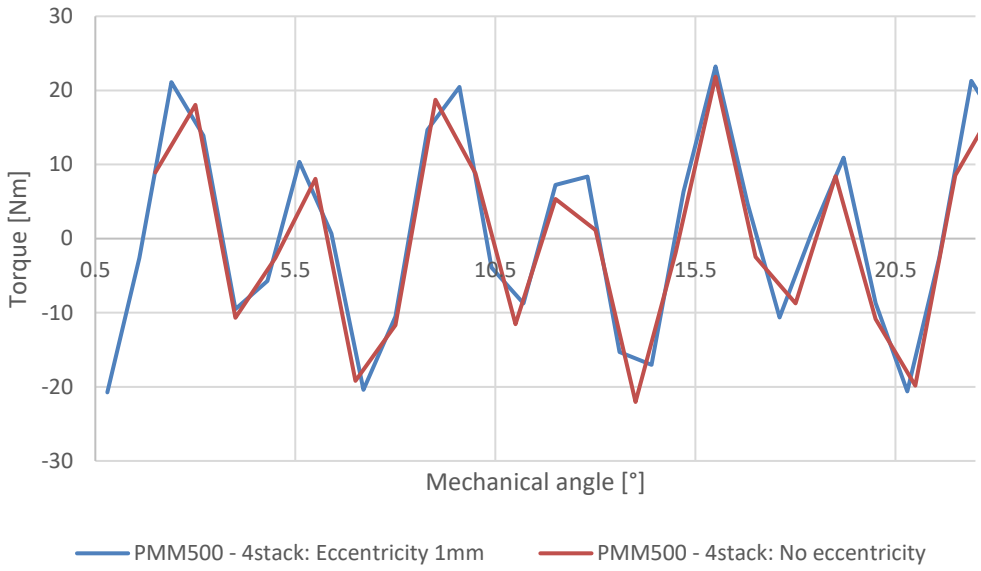

Figure 27: Torque of PMM500 machine with respect to mechanical angle.

Figure 27 shows the amplitude of the cogging torque. Time stepping was different for both cases as the time step was deemed too sparse in the earlier calculations, and some of the data with the higher time step got corrupted. The length of the time step was shortened to get better curves. The new time step was more frequent than the timestep during the 2D FEM model but still not enough to get an exact curve. Due to time constraints, calculations with shorter time steps or a better mesh could not be done. Due to the disparity between the results and the actual torque waveform, no conclusion can be made about the axial eccentricity's effect on the cogging torque.

6.2.4 The effect of axial eccentricity on the axial force

Axial eccentricity is the main reason for axial force. The axial force of the PMM500 machine is in Figure 28. Force in Figure 28 was modelled with a 4 stack model, and it depicts only one half of an electrical cycle.

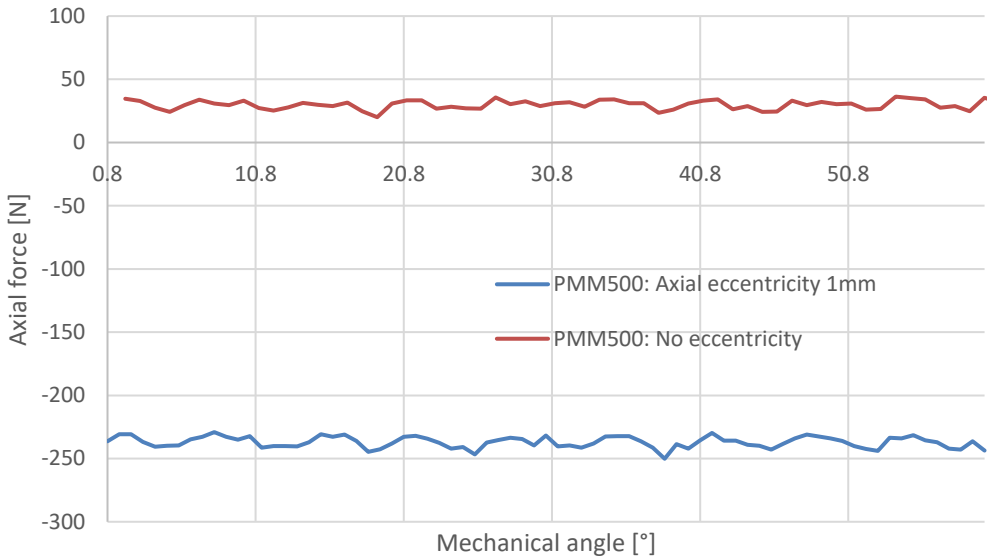

Figure 28: PMM500 machine's axial force during the non-eccentric condition and with 1 mm eccentricity.

Figure 28 shows that the axial force during non-eccentric condition is approximately 30 N and with 1 mm eccentricity -240 N. In an ideal situation, the axial force should be 0 N, but due to unevenness or too sparse mesh of the model, the force differs a bit. Eccentricity is induced towards the positive z-axis. For this reason, the force is negative as it counters eccentricity. For further comparison, the FFT of the axial force is in Figure 29.

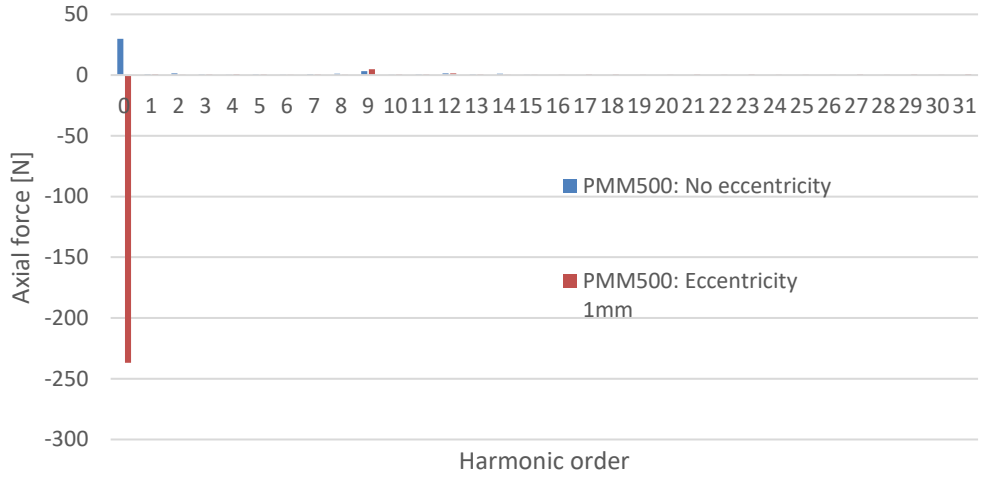

Figure 29: Axial force spectrum of PMM500 machine during the concentric condition and with 1mm eccentricity.

Due to there being an axial force already at the non-eccentric condition, the same force components can be seen in Figure 29 in the eccentric and non-eccentric conditions. Only one vibrational component can be seen at the 9th harmonic, which is caused by the stator slots. The vibration's amplitude is very small as the overall force is small, and the skewing decreases the amplitude of the vibration caused by the stator slots even further. Both the fundamental and harmonic components' amplitudes increase due to eccentricity, which follows the analysis done in subchapter 4.2.

Axial forces were calculated analytically based on the model created during this thesis and with the reference model based on Bradford and Rhudy [21]. Comparison between the calculated forces, measurements, and results obtained with FEM models with a reduced amount of stator stacks are compared in Figure 30, Figure 31, and Figure 32 for the full machine, 2 stacks and 4 stacks, respectively.

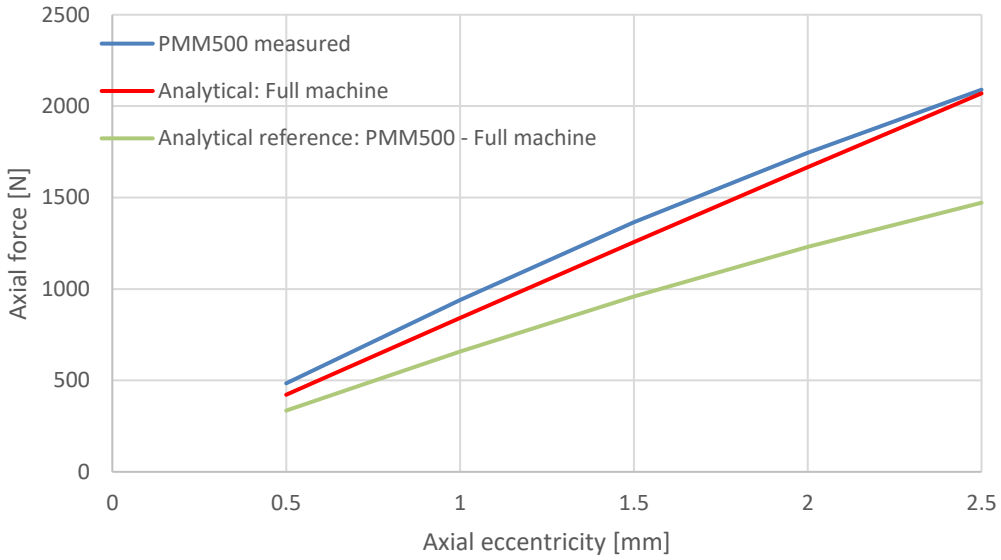

Figure 30: Axial force of a whole PMM500 machine with respect to eccentricity.

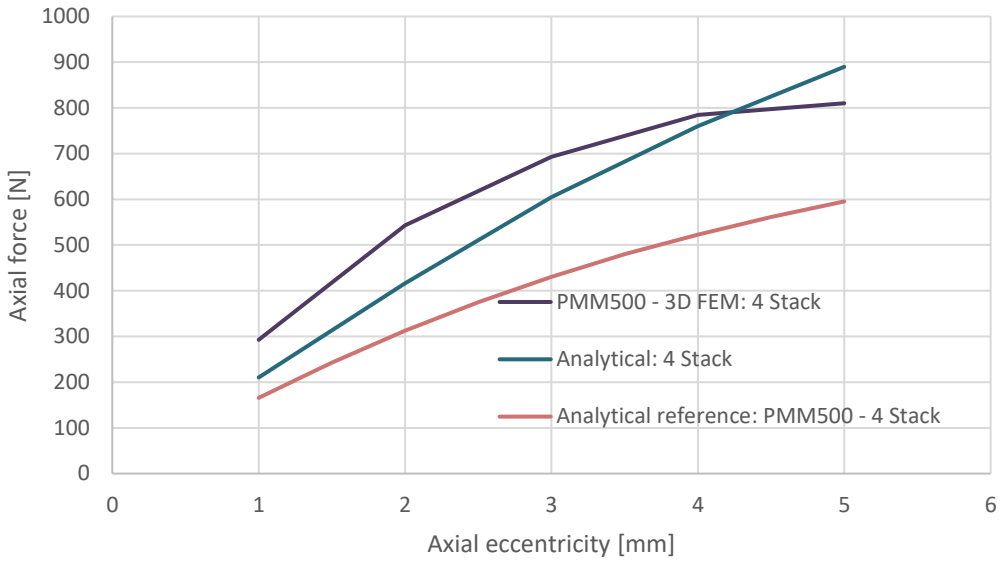

Figure 31: Axial force of 4 stacks of PMM500 machine with respect to eccentricity.

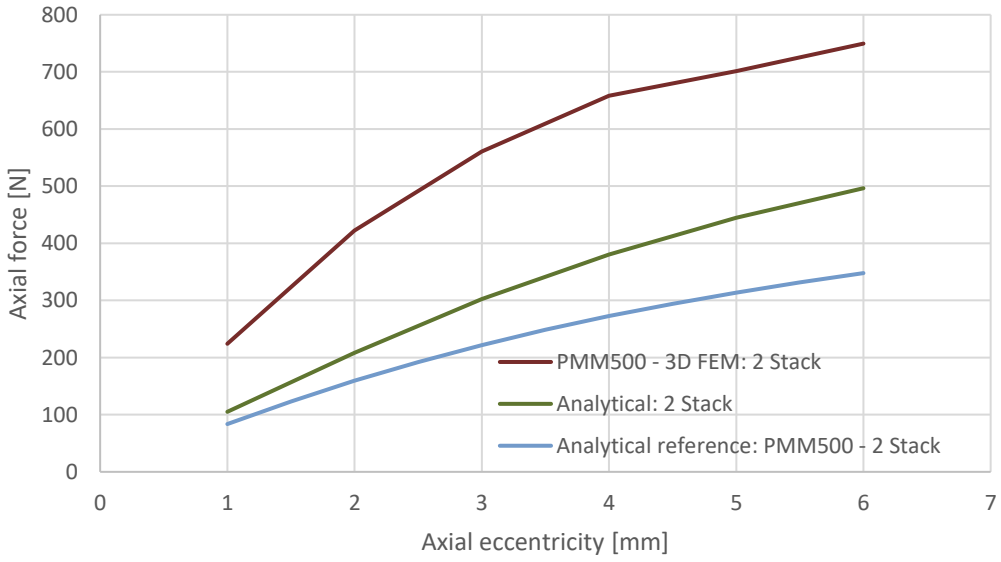

Figure 32: Axial force of 2 stacks of PMM500 machine with respect to eccentricity.

The figures show that the analytical model's accuracy increases when more stator stacks are included in the calculation. The comparison between the measured values and the analytical model is even closer than between FEM results and the analytical model. Still, the analytical model's values do not follow the curve of the FEM model or measurements that well. Results from 2 stack and 4 stack FEM models show that the curve starts to flatten around an eccentricity of 2.5 mm. The created analytical model was initially based on that the eccentricity would not increase so much that the magnet edge would go past the middle of the cooling duct. This would result in that part of the magnet would be closer to an-

other stator slot, which could change the flux flows and thus affect the created forces. Approximation was made that the flux flows would split based on the geometric centre between the stator stacks, which for the PMM500 machine is at 2.5 mm. The calculated axial force increases over the results of the FEM model. Thus, optimisation to the analytical model needs to be done. The created model calculates values are closer to the FEM results than the reference model by Bradford and Rhudy. Table 7 shows the values calculated with FEM and analytically and the percentual difference between the values.

Table 7: Comparison of analytical calculation results to measurements of the PMM500 machine.

Eccentricity: [mm]	PMM500 – Analytical: Full machine [N]	Difference:
0.5	421.62	12.89 %
1	841.02	10.53 %
1.5	1256.38	7.96 %
2	1666.43	4.50 %
2.5	2069.99	0.96 %

The linearity of the created model can be seen well in Table 7's results. The force increases approximately 420 N with every 0.5 mm increase, with a slight drop at the end. When these values are compared to the measured values, the overall difference becomes approximately 7.37 %. The main difference comes from the values of smaller eccentricities. For example, the actual difference at 0.5 mm is 16 N lower than at 2 mm, but the percentual difference is 7 % higher on the lower eccentricity. A similar comparison between 3D FEM results and an analytical model with a lower number of stacks yields overall percentual differences of 18.49 % and 38.38 % for models with 4 stacks and 2 stacks, respectively. These eccentricities are significantly higher. The forces calculated by the model are based on the number of stator stacks, which means that the force created by a single stack is multiplied by the number of stacks. This, compared with the results from FEM modelling, differs quite a lot. Axial force does not double with doubling size. Instead, the force increases faster and starts to saturate earlier, but the overall difference is only around 70 to 130 N, with 2 and 4 stack models. The model predicts that the force on all the stacks is the same, but in practice, flux flows change at the end of the machines.

Complete results of the PMM1500 axial force could not be modelled during this thesis. A single axial force obtained with the PMM1500 model was 179.6 N for 1 mm of eccentricity.

The axial force of the PMM1500 would be approximately 5064 N for 1 mm eccentricity with the analytical model created during this thesis and approximately 1400 N if only one magnet module would be included. Values obtained with the reference model for the same eccentricity are 290.8 N for a single magnet module and 1155.7 N for the whole machine. The reference model is closer to the result obtained with the FEM.

7. CONCLUSIONS

The scope of this thesis was to model electromagnetic forces of PMSMs during eccentric operation conditions and to review if 3D FEM modelling could be integrated to be a part of electrical modelling done at Yaskawa Lappeenranta. Forces were modelled with FEM, and the results were analysed based on a literature review. Furthermore, an analytical calculation tool was created based on the FEM calculations for axial force approximation based on machine properties. Both the amplitudes and the harmonic content of the forces were studied during normal and eccentric operation conditions. The main induced force components are the radial force for radial eccentricity and the axial force for axial eccentricity, but also effects for other components were evaluated. The findings of this study follow well the results of previous research, which was covered in chapters 2 to 4.

During this thesis, 5 different FEM models were created and run during various operating conditions. Both machines were modelled with a 2D radial and 3D models. 3D models did not include all the machine's sub stacks as the machine used to run the models could not do it. Instead, 2-stack and 4-stack models were created for PMM500, and one magnet module model was created for PMM1500. The forces calculated by these models are discussed in chapter 6. The main problems which arose during this study were the calculation time and the incapability of the software to model the complete machines. The meshing and the models were simplified as the calculations could not be done with the computer used during this project. Additionally, calculations took a significant amount of time, so optimisation of the process and the study of other operating conditions must be done during further research.

Previous research has found that the radial eccentricity changes the air gap permeance, which induces a radial force towards the air gap's minimum direction. Additionally, it increases the magnetic flux density and thus increases also the tangential and the axial force components within the system. The harmonic components are induced into the force. The results of this study follow mostly the results of previous research. Both the PMM500 and the PMM1500 machines' radial forces and harmonic amplitudes increased during the radial eccentricity. The most significant increase can be seen in the increase of the radial forces DC-component, but as the radial force increased due to the eccentricity, both machines' radial forces started to vibrate based on the stator slotting and the eccentricity.

Stator slotting's effect created a vibrating component, whose main vibrational order is a multiple of the stator slots. The eccentricity created a 2nd order harmonic component for the PMM500 machine. Additionally, the PMM500 machine's model had a rotating radial force component created during the non-eccentric condition, which can be seen in the 1st harmonic order. On the PMM1500 machine, the radial eccentricity also increased the cogging torque's amplitude. The PMM500 machine's amplitude of cogging torque decreased, which did not follow the results obtained during earlier research. The eccentricity caused additional harmonic components to both cogging torques. The harmonic orders induced by eccentricity are multiples of the number of poles in the machine. Thus, the main vibrational components caused by eccentricities were the 6th for the PMM500 machine and the 32nd for the PMM1500 machine if it is considered that only a quarter of the force wave was modelled for the PMM1500 machine.

Previous research has found that during axial eccentricity, the overall magnetic flux density decreases due to the reducing effective length of the machine. The change in axial direction also creates a magnetic potential difference between the ends of the machine, which means more energy is stored in the air gap, and this difference can be seen as an axial force. The results of this study follow well the results of previous research. Due to physical limitations and time constraints, axial eccentricity could not be thoroughly modelled for both machines. Thus, the results of the PMM1500 machine could not be presented within this thesis. The PMM500 model could be modelled, but only for 2- and 4-stack models. The axial eccentricity increased both the DC component and the amplitudes of axial force harmonics. Optimization could be further done for the created 3D models. The meshing and time-stepping could be improved further to optimise the results.

The analytical model created during this thesis could approximate the force of a whole PMM500 machine quite closely. The overall difference between FEM-modelling and analytical calculation was 7.37% for eccentricity values between 0.5 mm to 2.5 mm. The model was not based on previous research, and thus further confirmation for the calculations is required. If it can approximate the axial force of other machines, for example, the PMM1500 machine as closely, the results could be trusted better to calculate axial forces for different machine types. FEM modelling could be improved by creating full machine models of the PMM500 machine to verify the analytical model and the measurements. This requires a computer with significantly more memory and processing power than the computer used for the calculations during this thesis.

This thesis did not fully reach set goals. Creating multiple 3D FEM models took a significant portion of time, and even data of fully calculated models were lost due to errors with-

in the software used. For this reason, further research is deemed necessary. The literature review portion of this thesis is comprehensive. However, as no simple axial calculation model based on physical geometries was found during the research, a new one was created. Verification with different models is required to make any clear conclusion for the developed model's accuracy. Additionally, results of eccentricity's effects on cogging torque are incomprehensive, multiple sources were searched, but prior research explaining why the radial eccentricity increases the cogging torque on one machine and decreases on one machine could not be found. One of the goals of machine modelling is to reduce the cogging torque [9]. Thus, in ideal machines, the effects would become negligible. Created 3D models can be used to calculate other operating conditions. Thus, differences during load conditions and electromagnetic torque can be further researched.

REFERENCES

[1] L. Wu, H. Yin, D. Wang, Y. Fang, "On-Load Field Prediction in SPM Machines by a Subdomain and Magnetic Circuit Hybrid Model", *IEEE Transactions on Industrial Electronics*, 2020, 67(9):7190–201 Available from: https://ieeexplore.ieee.org/document/8848846/

[2] X. Wang, X. Sun, P. Gao, "Study on the effects of rotor-step skewing on the vibration and noise of a PMSM for electric vehicles", *IET Electric Power Applications*, 2020, 14(1):131–8 Available from: https://onlinelibrary.wiley.com/doi/10.1049/iet-epa.2019.0238

[3] X. Xu, Q. Han, F. Chu, "Review of Electromagnetic Vibration in Electrical Machines", *Energies*, 2018, 11(7):1779 Available from: https://doi.org/10.3390/en11071779

[4] I. Gómez, G. García, A. McCloskey, G. Almandoz, "Analytical Model to Calculate Radial Forces in Permanent-Magnet Synchronous Machines", *Applied Sciences*, 2021, 11(22):10865 Available from: https://doi.org/10.3390/app112210865

[5] A.J. Pina Ortega, L. Xu, "Investigation of Effects of Asymmetries on the Performance of Permanent Magnet Synchronous Machines", *IEEE Transactions on Energy Conversion*, 2017, 32(3):1002–11 Available from: https://ieeexplore.ieee.org/document/7880632/

[6] D.-J. Kim, H.-J. Kim, J.-P. Hong, C.-J. Park, "Estimation of Acoustic Noise and Vibration in an Induction Machine Considering Rotor Eccentricity", *IEEE Transactions on Magnetics*, 2014, 50(2):857–60 Available from: https://ieeexplore.ieee.org/document/6748930

[7] Y.-L. He, Y.-X. Sun, M.-X. Xu, X.-L. Wang, Y.-C. Wu, G. Vakil, et al., "Rotor UMP characteristics and vibration properties in synchronous generator due to 3D static air-gap eccentricity faults", *IET Electric Power Applications*, 2020, 14(6):961–71 Available from: https://onlinelibrary.wiley.com/doi/10.1049/iet-epa.2019.0844

[8] F. Lin, S. Zuo, X. Wu, "Electromagnetic vibration and noise analysis of permanent magnet synchronous motor with different slot-pole combinations", *IET Electric Power Applications*, 2016, 10(9):900–8 Available from: https://onlinelibrary.wiley.com/doi/10.1049/iet-epa.2016.0044

[9] J. Pyrhonen, V. Hrabovcova, T. Jokinen, "Design of rotating electrical machines", John Wiley & Sons, Incorporated, 2013, 615 p.

[10] A.J. Ali, A.H. Ahmed, B.M. Saied, "Cogging torque Mitigation for PMSM using stator slots design and Magnets skewing", In: 2019 2nd International Conference on Electrical, Communication, Computer, Power and Control Engineering (ICECCPCE), IEEE, 2019, p. 240–5 Available from: https://ieeexplore.ieee.org/document/9072908/

[11] Z. Xing, X. Wang, W. Zhao, "Cogging torque reduction based on segmented skewing magnetic poles with different combinations of pole-arc coefficients in surface-mounted permanent magnet synchronous motors", *IET Electric Power Applications*, 2021, 15(2):200–13 Available from: https://onlinelibrary.wiley.com/doi/full/10.1049/elp2.12026

[12] C. Zhao, S. Li, Y. Yan, "Influence factor analysis of PMSM air gap flux density", *2005 International Conference on Electrical Machines and Systems*, 2005, 1:334–9 Available from: http://ieeexplore.ieee.org/document/1574774/

[13] D. Zarko, D. Ban, T.A. Lipo, "Analytical calculation of magnetic field distribution in the slotted air gap of a surface permanent-magnet motor using complex relative air-gap permeance", *IEEE Transactions on Magnetics*, 2006, 42(7):1828–37 Available from: http://ieeexplore.ieee.org/document/1644900/

[14] K.-C. Kim, D.-H. Koo, J. Lee, "Analysis of Axial Magnetic Force Distribution Due to the Axial Clearance for Electrical Rotating Machine", *IEEE Transactions on Magnetics*, 2007, 43(6):2546–8 Available from: http://ieeexplore.ieee.org/document/4202804/

[15] Y.-L. He, M.-X. Xu, J. Xiong, Y.-X. Sun, X.-L. Wang, D. Gerada, et al., "Effect of 3D Unidirectional and Hybrid SAGE on Electromagnetic Torque Fluctuation Characteristics in Synchronous Generator", *IEEE Access*, 2019, 7:100813–23 Available from: https://ieeexplore.ieee.org/document/8766107/

[16] Z. Yang, W. Li, Y. Gou, T. Cai, "Research on Radial Force of Permanent Magnet Synchronous Motor Based on Maxwell", *Journal of Electrical Engineering & Technology*, 2020, 15(6):2601–8 Available from: https://doi.org/10.1007/s42835-020-00511-9

[17] Z.Q. Zhu, D. Howe, "Instantaneous magnetic field distribution in brushless permanent magnet DC motors. III. Effect of stator slotting", *IEEE Transactions on Magnetics*, 1993, 29(1):143–51 Available from: http://ieeexplore.ieee.org/document/195559/

[18] S. Zhu, W. Zhao, G. Liu, Y. Mao, Y. Sun, "Effect of Phase Shift Angle on Radial Force and Vibration Behavior in Dual Three-Phase PMSM", *IEEE Transactions on Industrial Electronics*, 2021, 68(4):2988–98 Available from: https://ieeexplore.ieee.org/document/9027127/

[19] "Global quantities available for postprocessing", cited 04/01/2022, Available from: https://2021.help.altair.com/2021.2/flux/Flux/Help/english/UserGuide/English/topics/GrandeursGlobalesDisponiblesALexploitationMT.htm

[20] J.Y. Song, K.J. Kang, C.H. Kang, G.H. Jang, "Cogging Torque and Unbalanced Magnetic Pull Due to Simultaneous Existence of Dynamic and Static Eccentricities and Uneven Magnetization in Permanent Magnet Motors", *IEEE Transactions on Magnetics*, 2016, 53(3):1–9 Available from: http://ieeexplore.ieee.org/document/7742931/

[21] C.E. Bradford, R.G. Rhudy, "Axial Magnetic Forces on Induction Machine Rotors [includes discussion]", *Transactions of the American Institute of Electrical Engineers Part III: Power Apparatus and Systems*, 1953, 72(3):488–94 Available from: http://ieeexplore.ieee.org/document/4498659/

[22] Y.-L. He, W.-Q. Deng, G.-J. Tang, "Analysis and Simulation on UMP and EMT Characters of Turbogenerator under Axial Air-Gap Eccentricity", *International Journal of Rotating Machinery*, 2015, 2015:1–10 Available from: http://www.hindawi.com/journals/ijrm/2015/825835/

[23] G.-J. Park, Y.-J. Kim, S.-Y. Jung, "Design of IPMSM Applying V-Shape Skew Considering Axial Force Distribution and Performance Characteristics According to the Rotating Direction", *IEEE Transactions on Applied Superconductivity*, 2016, 26(4):1–5 Available from: http://ieeexplore.ieee.org/document/7435282/

[24] A. Looser, T. Baumgartner, J.W. Kolar, C. Zwyssig, "Analysis and Measurement of Three-Dimensional Torque and Forces for Slotless Permanent-Magnet Motors", *IEEE Transactions on Industry Applications*, 2012, 48(4):1258–66 Available from: http://ieeexplore.ieee.org/document/6198889/

[25] L. Wu, H. Yin, D. Wang, Y. Fang, "On-Load Field Prediction in SPM Machines by a Subdomain and Magnetic Circuit Hybrid Model", *IEEE Transactions on Industrial Electronics*, 2020, 67(9):7190–201 Available from: http://ieeexplore.ieee.org/document/6718201/

[26] D.G. Dorrell, Min-Fu Hsieh, YouGuang Guo, "Unbalanced Magnet Pull in Large Brushless Rare-Earth Permanent Magnet Motors With Rotor Eccentricity", *IEEE Transactions on Magnetics*, 2009, 45(10):4586–9 Available from: http://ieeexplore.ieee.org/document/5257290/

[27] D. Guo, F. Chu, D. Chen, "The Unbalanced Magnetic Pull and Its Effects on Vibration in a Three-Phase Generator With Eccentric Rotor", *Journal of Sound and Vibration*, 2002, 254(2):297–312 Available from: https://linkinghub.elsevier.com/retrieve/pii/S0022460X0194088X